

# Thermodynamics and Constitution of Mg-Al-Ca-Sr-Mn Alloys: Part II. Procedure for Multicomponent Key Sample Selection and Application to the Mg-Al-Ca-Sr and Mg-Al-Ca-Sr-Mn Systems

A. Janz, J. Gröbner, and R. Schmid-Fetzer

(Submitted June 25, 2008; in revised form October 2, 2008)

A procedure is suggested to identify key sample compositions in  $n$ -component alloys, providing the most crucial information with limited experimental effort. The proposed algorithm furthermore establishes the exact type of reaction equation of the  $(n + 1)$  phase invariant equilibria. Predictive calculations of phase equilibria in quaternary Mg-Al-Ca-Sr and quinary Mg-Al-Ca-Sr-Mn alloys are performed based on elaborate binary and ternary thermodynamic descriptions. Experimental work, using key samples and Mg-rich alloys, demonstrates the viability of the current approach in validating the predictions. Finally, the impact of using more or less elaborate ternary data is quantitatively exemplified for the quinary system Mg-Al-Ca-Sr-Mn by a comparison of different thermodynamic data sets.

**Keywords** CALPHAD approach, experimental phase equilibria, invariant equilibria, liquidus surface, microstructure phase diagram

## 1. Introduction

Calcium and strontium are important components in advanced magnesium alloys, which are relevant for weight savings in the automotive industry or other applications as detailed in part I of this study.<sup>[1]</sup> Understanding the phase formation in Mg-Al-Ca-Sr (AXJ) alloys and modifications of Mg-Al-Zn (AZ) and Mg-Al-Mn (AM) alloys with Ca and/or Sr requires accurate knowledge about the interactions of all components in the various phases of the Mg-Al-Ca-Sr alloy system.

Adding small amounts of manganese to the Mg-Al-Ca-Sr system brings us to a more realistic approximation of *real* industrial alloys, since all commercial Mg-Al-based alloys contain small amounts of Mn. This is essential to improve the corrosion resistance. Free iron is transformed into Fe-Mn-(Al) compounds and thus rendered harmless.

The Calphad approach has been recognized as a powerful method to calculate the phase diagram and thermodynamic quantities for multicomponent systems with quite a high degree of accuracy. Importantly, the reliable thermodynamic calculation provides the basis for understanding multicomponent solidification behavior. In this broader sense, it is

A. Janz, J. Gröbner, and R. Schmid-Fetzer, Institute of Metallurgy, Clausthal University of Technology, Robert-Koch-Str. 42, D-38678 Clausthal-Zellerfeld, Germany. Contact e-mail: schmid-fetzer@tu-clausthal.de.

termed Computational Thermodynamics and has proven to be a powerful tool for focused development of alloys<sup>[2]</sup> and optimization of processing conditions during casting and heat treatment,<sup>[3]</sup> limiting process temperatures in metal forming,<sup>[4]</sup> and so on.

A reliable thermodynamic database is required to secure the quality of such calculations. The purpose of part I of this study was to generate a consistent thermodynamic description of the phase equilibria in the two ternary systems Mg-Ca-Sr and Al-Ca-Sr by combining experimental work with thermodynamic modeling.<sup>[1]</sup> This filled the gap to approach the quaternary Mg-Al-Ca-Sr alloy system since the two other ternaries, Mg-Al-Ca and Mg-Al-Sr, have been recently completed.<sup>[1,5]</sup>

The purpose of the present part II of this study is to establish experimental validation of predictive calculations of phase equilibria, which are performed in quaternary Mg-Al-Ca-Sr and quinary Mg-Al-Ca-Sr-Mn alloys. A concise algorithm is developed to identify key sample compositions in  $n$ -component alloys, providing the most crucial information with limited experimental effort. This is of the utmost importance in coping with the overwhelming scale of possible experimentation in systems with four or five components.

## 2. Procedure for Key Sample Selection and Determination of Invariant Reactions

Given a draft phase diagram, either estimated or by predictive thermodynamic calculations, what are the key experiments to validate or improve these phase diagram data? To be more specific with this generic problem, let us focus on the investigation of phase boundaries with thermal analysis (differential scanning calorimetry, or DSC, or

differential thermal analysis, or DTA), which may be complemented by subsequent microstructure analysis. Thus, what are the *key sample* compositions providing the most crucial information or the maximum return on the investment of experimental resources?

The temperature of invariant reactions is well known to be among the most decisive data, especially if combined with a thermodynamic calculation of the phase diagram. Furthermore, this quantity is favorably measured since the invariant temperature does not change over a certain composition range and is often less influenced by side effects such as supercooling. Other phase boundaries, for example the liquidus temperature, are much more prone to experimental errors.

Selecting such key samples is rather straightforward for binary systems, partially manageable for ternary systems, but increasingly complex for systems with four or even more components. For example, in a binary system with a eutectic one would choose a sample with the estimated eutectic liquid composition since this sample would provide the maximum heat effect due to an exhaustive reaction, thus promising the maximum thermal analysis signal.

Guided by this idea a procedure has been developed to determine the analogous centroid sample composition for any type of invariant reaction in any multicomponent system. This sample will give the maximum possible amount of heat exchange for this reaction, assuming a kinetic completion of the invariant reaction. Since we are concerned with at least ternary, but essentially quaternary or higher component systems, the procedure will be linked to a thermodynamic calculation as the indispensable tool for a quantitative treatment of such systems. This is in line with a state-of-the-art iterative improvement of a thermodynamic dataset based on the results of selected experiments.

Therefore, it is assumed that a (preliminary) thermodynamic description of the  $n$ -component system is available and also software (such as Pandat<sup>[6]</sup>) providing at each isobaric  $(n + 1)$  phase invariant reaction the temperature,  $T_{inv}$ , and compositions  $x_i^\phi$  of all involved phases  $\phi$  and components  $i$ ,  $i = 1 \dots n$ . Constant pressure is considered throughout. It is not necessary to know the actual reaction equation, rather this will be also a result of the algorithm.

This procedure was developed for any invariant reaction in any multicomponent alloy. An explicit example is given at the end of this section for the quinary key sample MACSM1. The procedure is visualized with the example of a three-component, four-phase invariant equilibrium of the transition type with the reaction



The compositional location of these phases is presented in Fig. 1, and  $L + \alpha$  are denoted as educts (ed) and  $\beta + \gamma$  as products (prod).

### 2.1 Step 1: Average Composition

In the first step one has to get an alloy with a composition somewhere *inside* the invariant equilibrium field, depicted as “1” in Fig. 1. It is suggested that the simplest option be used; this is the calculation of the average composition of

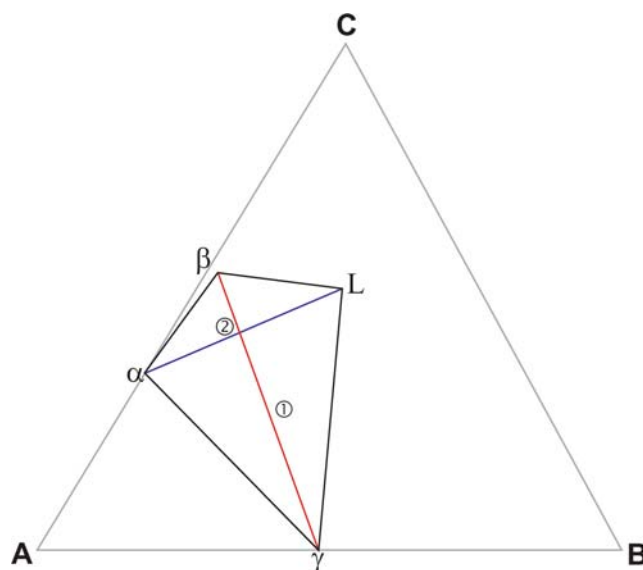


Fig. 1 Schematic view of a transition type invariant four-phase reaction in a ternary composition triangle of an A-B-C system

phases,  $\bar{x}_i$ , for all components  $i$  using the arithmetic mean of the compositions  $x_i^\phi$  of all the involved phases  $\phi$ . Any other composition somewhere inside the space spanned by the  $(n + 1)$  phase would also be suitable as alloy 1 for the next step.

### 2.2 Step 2: Phase Fraction Increments and Reaction Equation

In the second step, we have to find out the amounts of phases converted in the invariant reaction. This is done by probing the phase equilibria slightly above and below  $T_{inv}$ . In practice one performs a line calculation, scanning the temperature in small steps at fixed composition of alloy 1. This also reveals possible interference of another nearby invariant reaction. Using the composition  $\bar{x}_i$  of alloy 1 for these calculations is more general than taking the composition of the liquid phase  $L$ , which may be just scratching on the equilibrium space, as depicted in Fig. 1. Only for the special case of eutectic reactions would this work out, but not for peritectic or transition type reactions.

At each isobaric  $(n + 1)$  phase invariant reaction, we have the intersection of  $(n + 1)$  different monovariant  $n$ -phase equilibria. Slightly above the invariant reaction,  $T_{inv} + \delta T$ , there are  $k$  of these and slightly below,  $T_{inv} - \delta T$ , there are  $(n + 1 - k)$ . In the example of Fig. 1, there are two-three-phase equilibria above and two other below  $T_{inv}$ .

Since the composition of alloy 1 is inside the  $(n + 1)$  phase space, it will generally probe one  $n$ -phase equilibrium out of the  $k$  possible ones at  $T_{inv} + \delta T$  and a *different*  $n$ -phase equilibrium below. Thus, information is provided on the growth/shrinkage of *all* the  $(n + 1)$  phases by just these two probing calculations, even though  $(n + 1)$  different monovariant  $n$ -phase equilibria exist.

At both probing points,  $T_{inv} + \delta T$  and  $T_{inv} - \delta T$  at composition 1, the equilibrium phase fractions are well

defined and obtained by the thermodynamic calculation; the sum of all phase fractions at each point is equal to 1:

$$\sum_{j=1}^n f^{\phi_j} = 1 \quad (\text{Eq 2})$$

Furthermore the difference between the fractions of each participating phase  $\phi$  that is converted in the invariant reaction is

$$\Delta f^{\phi} = f^{\phi, \text{after\_reaction}} - f^{\phi, \text{before\_reaction}} \quad \text{for } \phi = 1, \dots, n+1 \quad (\text{Eq 3})$$

It is emphasized again that, starting with  $n$  phases above the invariant, one additional phase must appear at  $T_{\text{inv}}$  and a *different* phase must disappear when cooling to  $T_{\text{inv}} + \delta T$ . Therefore, Eq 3 provides information about *all*  $n+1$  phases in the invariant reaction, irrespective of the selection of the specific  $n$ -phase equilibrium at  $T_{\text{inv}} + \delta T$ . The mass balance requires the following to be true:

$$\sum_{\phi=1}^{n+1} \Delta f^{\phi} = \sum_{\phi=1}^{n+1} f^{\phi, \text{after\_reaction}} - \sum_{\phi=1}^{n+1} f^{\phi, \text{before\_reaction}} = 1 - 1 = 0 \quad (\text{Eq 4})$$

We define educts and products by  $\Delta f^{\phi, \text{ed}} < 0$  and  $\Delta f^{\phi, \text{prod}} > 0$ . Sorting according to negative and positive phase fraction increments gives the actual invariant reaction equation with proper fractions

$$\phi_1^{\text{ed}} + \phi_2^{\text{ed}} + \dots + \phi_k^{\text{ed}} = \phi_{k+1}^{\text{prod}} + \phi_{k+2}^{\text{prod}} + \dots + \phi_{n+1}^{\text{prod}} \quad (\text{Eq 5})$$

Based on the definitions above it is obvious that

$$\left| \sum_{j=1}^k \Delta f^{\phi_{j, \text{ed}}} \right| = \left| \sum_{j=k+1}^{n+1} \Delta f^{\phi_{j, \text{prod}}} \right| \quad (\text{Eq 6})$$

It is emphasized that at this point the exact invariant type of reaction is uniquely given by the sorting scheme in Eq 5, simply based on the signs of  $\Delta f^{\phi}$ . Another method to determine the  $(n+1)$  phase invariant reaction equation is to consider *all*  $(n+1)$  different monovariant  $n$ -phase equilibria using a Scheil reaction scheme.<sup>[7]</sup> This is easy for a ternary system, but becomes increasingly complex for multicomponent systems. By contrast, the proposed algorithm requires only two simple point calculations, involving only *two* of the  $n$ -phase equilibria. The result is certain since it is based on the unquestionable materials balance of the reaction. The only potential failure of the algorithm is expected if the probing composition of alloy 1 by coincidence falls exactly on a lower dimensional  $(n-1)$  phase equilibrium. In the example of Fig. 1, this is a location exactly on the line  $\beta$ - $\gamma$  or the line  $L$ - $\alpha$ . Such degeneracy is easily corrected by a small composition shift.

### 2.3 Step 3: Alloy Composition for Key Sample

In the third step, we get the composition of alloy 2 with the maximum (completely) converted phase amounts,

$x_i^{\text{Alloy2}}$ . This is the desired key sample composition that will produce the complete invariant reaction: all the educt phases are fully converted to the product phases.

It is essential that the differences of the phase fractions are normalized to sum up to unity on each side of the reaction:

$$\Delta f^{\phi_{m, \text{ed}-N}} = \frac{\Delta f^{\phi_{m, \text{ed}}}}{\left| \sum_{j=1}^k \Delta f^{\phi_{j, \text{ed}}} \right|} \quad \text{for } m = 1, \dots, k \quad (\text{Eq 7})$$

$$\Delta f^{\phi_{m, \text{prod}-N}} = \frac{\Delta f^{\phi_{m, \text{prod}}}}{\left| \sum_{j=k+1}^{n+1} \Delta f^{\phi_{j, \text{prod}}} \right|} \quad \text{for } m = k+1, \dots, n+1 \quad (\text{Eq 8})$$

According to the reaction in Eq 5 we thus get a normalized version of Eq 6 for the converted phase fractions:

$$1 = \left| \Delta f^{\phi_{1, \text{ed}-N}} \right| + \left| \Delta f^{\phi_{2, \text{ed}-N}} \right| + \dots = \left| \Delta f^{\phi_{1, \text{prod}-N}} \right| + \left| \Delta f^{\phi_{2, \text{prod}-N}} \right| + \dots \quad (\text{Eq 9})$$

The centroid composition of the invariant reaction,  $x_i^{\text{Alloy2}}$ , can be calculated as a weighed average of educt composition (or alternatively, product composition):

$$x_i^{\text{Alloy2}} = \sum_{j=1}^{\text{educts}} \left( x_i^{\phi_{j, \text{ed}}} \cdot \Delta f^{\phi_{j, \text{ed}-N}} \right) = \sum_{j=k+1}^{\text{products}} \left( x_i^{\phi_{j, \text{prod}}} \cdot \Delta f^{\phi_{j, \text{prod}-N}} \right) \quad \text{for } i = 1, \dots, n \quad (\text{Eq 10})$$

Furthermore, the combined information on the centroid composition and the normalized converted phase fractions is most useful for a screening of all the calculated invariant reactions to distinguish relevant from irrelevant reactions. Reactions that essentially degenerate to some lower-order subsystem are considered irrelevant since they do not provide information about the  $n$ -component system but only about one of the  $(n-1)$  component subsystems. These lower-order subsystems are assumed to have been studied separately beforehand, possibly using the same procedure. Such degenerate/irrelevant invariant reactions can be recognized by showing at least one of the normalized phase fractions very close to zero and/or the centroid composition very close to one of the edge subsystems; typically the reaction temperature is also close to a corresponding invariant reaction in the  $(n-1)$  component subsystem. For example, the measurement of a ternary four-phase reaction that is essentially degenerate to a binary three-phase eutectic will not provide useful information for a quantitative validation of the ternary liquid phase interactions.

Moreover, the centroid compositions may be useful for an additional screening according to the region of interest. It is unlikely that one needs to investigate the entire composition space of a quinary system such as Mg-Al-Ca-Sr-Mn with the same degree of accuracy; certainly one would not receive external funding for that. Currently we are interested

## Section I: Basic and Applied Research

in Mg-based alloys and may focus on Mg-rich reactions. Again, this means the centroid composition, not the liquid composition. These two compositions are only identical for a true eutectic reaction. Experience shows that this eutectic reaction type becomes scarce with increasing number of components. For example, only 1 out of 46 invariant reactions involving the liquid phase in the Mg-Al-Ca-Sr-Mn system is a true eutectic; all the other 45 are transition-type (U-type) reactions.

In addition to considering only the reactions with a Mg-rich centroid composition one may further focus on reactions involving both the liquid and the (Mg) solid-solution phase since this phase must occur in any microstructure of interest for Mg-based alloys. For example, in the Mg-Al-Ca-Sr-Mn system there are 12 out of 46 invariant reactions involving (Mg) and liquid. Of these 12, there are 6 that degenerate to the quaternary Mg-Al-Ca-Sr edge system with reaction temperatures differing by less than 0.03 K. Considering only the nondegenerate Mg-rich reactions leaves only two reactions worthy of experimental validation;

these correspond to the quinary key samples MACSM1 and MACSM2 as detailed below.

For example, sample MACSM1 was selected at the centroid composition of the six-phase invariant reaction 5cU20 at  $T_{inv} = 490$  °C:  $L + Al_8Mn_5 \leftrightarrow (Mg) + C15 + Al_4Sr + Al_{11}Mn_4$ . In step 1 of the procedure the average composition of participating phases is calculated as given in Table 1(a). This defines “Alloy 1,” which is then used in step 2 to calculate the phase amounts above and below  $T_{inv}$ . These are given in Table 1(b) in the second and third line for  $T_{inv} + \delta T$  and  $T_{inv} - \delta T$ , respectively. The sign of the difference in the fourth line indicates the educt phases  $L + Al_8Mn_5$  (negative, decreasing amount) and the product phases  $(Mg) + C15 + Al_4Sr + Al_{11}Mn_4$  (positive, increasing amount). The normalized difference is then used in step 3 to calculate the weighted compositions in Table 1(c). These are the contributions to “Alloy 2,” which is the centroid composition and, thus, the key sample MACSM1. The same result is of course obtained from the weighted compositions of either the two educt phases or the four product phases.

**Table 1 (a) Step 1—Phase compositions at invariant reaction 5cU20. (b) Step 2—Phase amounts in “Alloy 1,” the average composition of Table 1(a), calculated 0.01 °C above and below  $T_{inv}(5cU20) = 490.22$  °C; molar fractions. (c) Step 3—Weighted compositions, contributing to “Alloy 2,” the centroid composition of 5cU20, thus defining key sample MACSM1**

Phase	Composition, at.%					
	Al	Ca	Mg	Mn	Sr	
<b>(a) Step 1</b>						
Liquid	23.5695	3.1339	72.6441	0.0078	0.6447	
$Al_8Mn_5$	58.8327	0	0	41.1673	0	
(Mg)	5.5718	0.0096	94.4146	0.0027	0.0012	
C15	64.7267	32.0454	1.9400	0	1.2879	
$Al_4Sr$	72.7945	0.0978	7.2055	0	19.9022	
$Al_{11}Mn_4$	73.3333	0	0	26.6667	0	
Average	49.80	5.88	29.37	11.31	3.64	
	<b>Liquid</b>	<b><math>Al_8Mn_5</math></b>	<b>(Mg)</b>	<b>C15</b>	<b><math>Al_4Sr</math></b>	<b><math>Al_{11}Mn_4</math></b>
<b>(b) Step 2</b>						
490.23 °C	0.384451	0.21129	0	0.145398	0.161031	0.097829
490.21 °C	0	0.132921	0.294262	0.182879	0.171043	0.218895
Difference	-0.384451	-0.078369	0.294262	0.037481	0.010012	0.121066
Normalized difference	-0.8307	-0.1693	0.6358	0.0810	0.0216	0.2616
	Composition, at.%					
	Al	Ca	Mg	Mn	Sr	
<b>(c) Step 3</b>						
Liquid	19.58	2.60	60.34	0.01	0.54	
$Al_8Mn_5$	9.96	0	0	6.97	0	
Total educts	29.54	2.60	60.34	6.98	0.54	
(Mg)	3.54	0.01	60.02	0.00	0.00	
C15	5.24	2.59	0.16	0	0.11	
$Al_4Sr$	1.58	0.00	0.16	0	0.43	
$Al_{11}Mn_4$	19.18	0	0	6.98	0	
Total products	29.54	2.60	60.34	6.98	0.54	

The resulting composition of “Alloy 2,” Al<sub>29.54</sub>-Ca<sub>2.60</sub>-Mg<sub>60.34</sub>-Mn<sub>6.98</sub>-Sr<sub>0.54</sub> (at.%), converts to Al<sub>28.48</sub>-Ca<sub>3.72</sub>-Mg<sub>52.40</sub>-Mn<sub>13.70</sub>-Sr<sub>1.69</sub> (wt.%). This is slightly different from the actual composition of MACSM1 given in Table 2. The reason is that at the beginning of our research the key samples were calculated with an earlier thermodynamic dataset of the Mg-Al-Mn system.<sup>[8]</sup> The compositions given in Table 1(a) to (c) can be reproduced with the current thermodynamic description. A similar shift occurred with sample MACSM2.

Similarly, in the Mg-Al-Ca-Sr system there are 6 out of 24 invariant reactions involving (Mg) and liquid. Considering only the nondegenerate Mg-rich reactions leaves again only two reactions worth of experimental validation; these correspond to the quaternary key samples MACS1 and MACS2 as detailed below. By the way, only 1 of the 24 invariants is a eutectic reaction.

These examples highlight the enormous potential of the suggested procedure to focus limited experimental resources

on the investigation of most decisive invariant reactions and the selection of key samples in multicomponent alloy systems. In a refinement of this procedure, it was checked in preliminary calculations if other thermal signals are expected for this sample very close to the temperature of the aimed invariant reaction. If this is the case, the peaks might not be separated properly. Simulating the solidification of the sample using different cooling conditions (equilibrium, Scheil) may indicate if the sample composition should be shifted.

### 3. Experimental Work

#### 3.1 Sample Preparation and Analysis

Using the algorithm presented above, two Mg-Al-Ca-Sr key samples were selected to assess the accuracy of the

**Table 2** Temperatures extracted from the DTA curves obtained by thermal analysis in the Mg-Al-Ca-Sr-Mn system and their interpretation. Invariant reactions were recognized from the peak shape

No.	Sample composition, wt.%	Thermal signal, °C			Interpretation Calculated equilibrium temperature, °C; Phase boundary or invariant reaction
		Heating(a)	Cooling(b)	Evaluated	
MRI135	Mg90.53	...	...	...	642 L/L + Al <sub>8</sub> Mn <sub>5</sub>
	Al8.00	604 s	602 s	604	604 L + Al <sub>8</sub> Mn <sub>5</sub> /L + Al <sub>8</sub> Mn <sub>5</sub> + (Mg)
	Ca1.01	506 s	504 s	506	503 L + Al <sub>8</sub> Mn <sub>5</sub> + (Mg)/L + Al <sub>8</sub> Mn <sub>5</sub> + (Mg) + C15
	Sr0.24	...	...	...	493 L + Al <sub>8</sub> Mn <sub>5</sub> + (Mg) + C15/L + Al <sub>8</sub> Mn <sub>5</sub> + (Mg) + C15 + Al <sub>4</sub> Sr
	Mn0.22	...	...	...	<b>490 5cU20</b>
MRI230	Mg91.92	...	...	...	487 L + (Mg) + C15 + Al <sub>4</sub> Sr + Al <sub>11</sub> Mn <sub>4</sub> /(Mg) + C15 + Al <sub>4</sub> Sr + Al <sub>11</sub> Mn <sub>4</sub>
	Al6.16	612 s	606 s	612	634 L/L + Al <sub>8</sub> Mn <sub>5</sub>
	Ca1.49	522 s	522 s	622	612 L + Al <sub>8</sub> Mn <sub>5</sub> /L + Al <sub>8</sub> Mn <sub>5</sub> + (Mg)
	Sr0.21	...	...	...	519 L + Al <sub>8</sub> Mn <sub>5</sub> + (Mg)/L + Al <sub>8</sub> Mn <sub>5</sub> + (Mg) + C36
	Mn0.22	...	...	...	511.2 L + Al <sub>8</sub> Mn <sub>5</sub> + (Mg) + C36/L + Al <sub>8</sub> Mn <sub>5</sub> + (Mg) + C36 + C15
MACSM1	Mg47.73	...	...	...	511.0 L + Al <sub>8</sub> Mn <sub>5</sub> + (Mg) + C36 + C15/L + Al <sub>8</sub> Mn <sub>5</sub> + (Mg) + C15
	Al31.21	517 s	515 w	517	505 L + Al <sub>8</sub> Mn <sub>5</sub> + (Mg) + C15/Al <sub>8</sub> Mn <sub>5</sub> + (Mg) + C15
	Ca3.37	507	512	507	L/L + Al <sub>8</sub> Mn <sub>5</sub>
	Sr1.85	...	...	...	527 L + Al <sub>8</sub> Mn <sub>5</sub> /L + Al <sub>8</sub> Mn <sub>5</sub> + Al <sub>11</sub> Mn <sub>4</sub>
	Mn15.83	489 s	499 s	490	507 L + Al <sub>8</sub> Mn <sub>5</sub> + Al <sub>11</sub> Mn <sub>4</sub> /L + Al <sub>8</sub> Mn <sub>5</sub> + Al <sub>11</sub> Mn <sub>4</sub> + Al <sub>4</sub> Sr
MACSM2	Mg76.57	...	...	...	490.4 L + Al <sub>8</sub> Mn <sub>5</sub> + Al <sub>11</sub> Mn <sub>4</sub> + Al <sub>4</sub> Sr/L + Al <sub>8</sub> Mn <sub>5</sub> + Al <sub>11</sub> Mn <sub>4</sub> + Al <sub>4</sub> Sr + (Mg)
	Al 2.36	...	512 w	521	<b>490 5cU20</b>
	Ca11.96	514 w	513 w	514	484 L + Al <sub>11</sub> Mn <sub>4</sub> + Al <sub>4</sub> Sr + (Mg) + C15/Al <sub>11</sub> Mn <sub>4</sub> + Al <sub>4</sub> Sr + (Mg) + C15
	Sr 8.31	...	...	...	?
	Mn 0.80	...	...	...	L/L + Al <sub>8</sub> Mn <sub>5</sub>
		505 s	505 s	505	?
					514 L + Al <sub>8</sub> Mn <sub>5</sub> /L + Al <sub>8</sub> Mn <sub>5</sub> + Mg <sub>17</sub> Sr <sub>2</sub>
					512.1 L + Al <sub>8</sub> Mn <sub>5</sub> + Mg <sub>17</sub> Sr <sub>2</sub> /L + Al <sub>8</sub> Mn <sub>5</sub> + Mg <sub>17</sub> Sr <sub>2</sub> + (Mg)
					511.59 L + Al <sub>8</sub> Mn <sub>5</sub> + Mg <sub>17</sub> Sr <sub>2</sub> + (Mg)/L + Al <sub>8</sub> Mn <sub>5</sub> + Mg <sub>17</sub> Sr <sub>2</sub> + (Mg) + C14
					511.55 L + Al <sub>8</sub> Mn <sub>5</sub> + Mg <sub>17</sub> Sr <sub>2</sub> + (Mg) + C14/Al <sub>8</sub> Mn <sub>5</sub> + Mg <sub>17</sub> Sr <sub>2</sub> + (Mg) + C14

(a) Onset for invariant reactions, peak maximum otherwise

(b) Onset. w, weak and diffuse signal; s, strong and clear signal; ..., not detected; ?, not assigned

**5cU20** at 490 °C: L + Al<sub>8</sub>Mn<sub>5</sub> ↔ (Mg) + C15 + Al<sub>4</sub>Sr + Al<sub>11</sub>Mn<sub>4</sub>

## Section I: Basic and Applied Research

calculated invariant five-phase reactions involving both the liquid and the (Mg) phase and having a Mg-rich overall composition. The compositions of these centroid alloy samples are given in Table 3. The sample preparation in sealed tantalum capsules is described in part 1 of this paper<sup>[1]</sup>; differential thermal analysis was performed with three consecutive heating/cooling cycles with 5 K/min first followed by three cycles at 1 K/min. Sample MACS1 was analyzed within the temperature range of 300 to 600 °C (400 to 700 °C for sample MACS2).

Two of the four quinary samples were machined out of commercial alloy material (MRI135 and MRI230) from Dead Sea Magnesium Ltd. (Beer Sheva, Israel). The chemical composition of these alloys was analyzed by ICP-AES from the corresponding blooms: Mg-8.00Al-1.01Ca-0.24Sr-0.22Mn-0.027Na-0.0076K-0.0026Fe-0.00017Be (wt.%) (MRI 153) and Mg-6.16Al-1.49Ca-0.21Sr-0.22Mn-0.028Na-0.0073K-0.0015Fe-0.00022Be (wt.%) (MRI230).

The compositions of the two additional quinary key samples were selected using the algorithm given above to find the centroid alloy composition. Again, only those six-phase invariant reactions were considered involving the (Mg) phase. The thermodynamic dataset used for the selection of the quinary key samples comprised the Mg-Al-Mn system as assessed by Ohno Schmid-Fetzer.<sup>[8]</sup> The sample MACSM1 was selected at the centroid of the calculated U-type reaction  $5cU20: L + Al_8Mn_5 \leftrightarrow (Mg) + C15 + Al_4Sr + Al_{11}Mn_4$ , and sample MACSM2 at  $5cU13: L + Al_8Mn_5 \leftrightarrow C14 + Mg_{17}Sr_2 + \alpha Mn + (Mg)$ . The samples were prepared from high-purity metals just like the quaternary synthetic samples. The manganese used in these experiments was supplied by Chempur (Karlsruhe, Germany) with 0.8 to 3 mm shot size and a purity of 99.99% Mn.

After testing the tightness of the Ta capsules, differential thermal analysis was again performed using the procedure described previously within a temperature range estimated by the thermodynamic calculations. Table 2 compiles the quinary sample compositions, as also used for the

thermodynamic calculations, together with the results of the DTA investigation.

After slow cooling in the last cooling cycle of thermal analysis, the microstructures of all samples were investigated using backscattered electron contrast in scanning electron microscopy (SEM/BSE). Local compositions were analyzed with EDX. Phase identification based on the local chemical composition turned out to be difficult since the microstructure of some phases was very fine. In general, the chemical composition of C36 and C15 are very similar. It is difficult to distinguish between these phases with EDX or even with EPMA in the multicomponent alloy systems especially if very fine microstructures evolved. More detailed investigations with TEM, out of the scope of this study, would be required for an improved phase analysis, such as has been done for the Mg-Al-Ca system.<sup>[9,10]</sup>

### 3.2 Experimental Results

Results of the DTA investigation are presented in Table 2 and 3 for the quinary and quaternary samples, respectively.

The four-phase microstructure of the quaternary sample MACS1 is presented in Fig. 2. Two phases appear as large grains: the  $Mg_{17}Sr_2$  and the C15- $Al_2Ca$  phase. Furthermore, smaller single phase regions of (Mg), and two different fine lamellar two-phase regions involving (Mg) can be found. The brighter lamellas were identified by EDX as  $Al_4Sr$ , whereas the darker lamellas are C15. The EDX analysis was performed in other parts of this sample where coarser areas of (Mg), (Mg) + C15 and (Mg) +  $Al_4Sr$  exist. From this microstructure it is clear that the primary crystallizing phase is either  $Mg_{17}Sr_2$  or C15- $Al_2Ca$ .

Figure 3 shows the microstructure of sample MACS2; primary (Mg) dominates the image of this more Mg-rich alloy. Additionally, C36 has grown between the (Mg) grains. A fine-structured eutectic completes the solidification structure, denoted as (Mg) + X as discussed later.

**Table 3** Temperatures extracted from the DTA curves obtained by thermal analysis in the Mg-Al-Ca-Sr system and their interpretation

No.	Sample composition, wt.%	Thermal signal, °C			Interpretation Calculated equilibrium temperature, °C; Phase boundary or invariant reaction
		Heating(a)	Cooling(b)	Evaluated	
MACS1	Mg65.83	538 w	525 w	538	537 L/L + $Mg_{17}Sr_2$
	Al19.4	...	...	...	522 L + $Mg_{17}Sr_2/L + Mg_{17}Sr_2 + Al_4Sr$
	Ca5.13	505 s	501 s	505	<b>505 U8</b>
	Sr9.64	...	...	...	504 L + $Al_4Sr + C15 + (Mg)/Al_4Sr + C15 + (Mg)$
MACS2	Mg91.63	...	609 w	609	609 L + (Mg)
	Al4.79	517 s	524 s	519	523 L + (Mg)/L + (Mg) + C36
	Ca3.23	...	...	...	510 L + (Mg) + C36/L + (Mg) + C36 + C14
	Sr0.35	507 s	509 s	508	<b>508 E1</b>

(a) Onset for invariant reactions, peak maximum otherwise

(b) Onset. w, weak and diffuse signal; s, strong and clear signal; ..., not detected

Invariant reactions were recognized from the peak shape

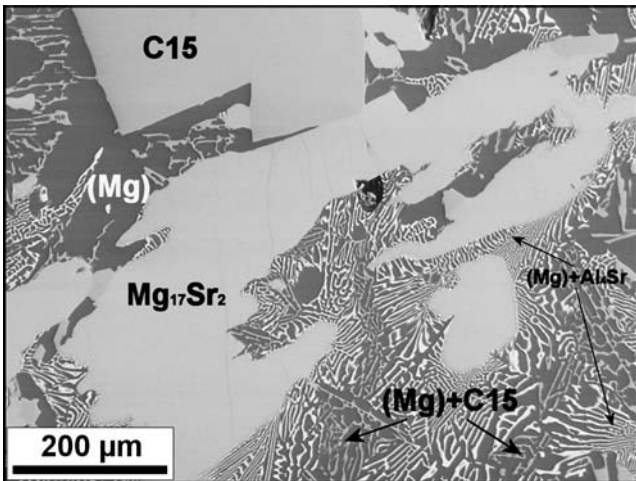


**Fig. 2** Scanning electron micrograph (SEM/BSE) of sample MACS1 after slow cooling in DTA

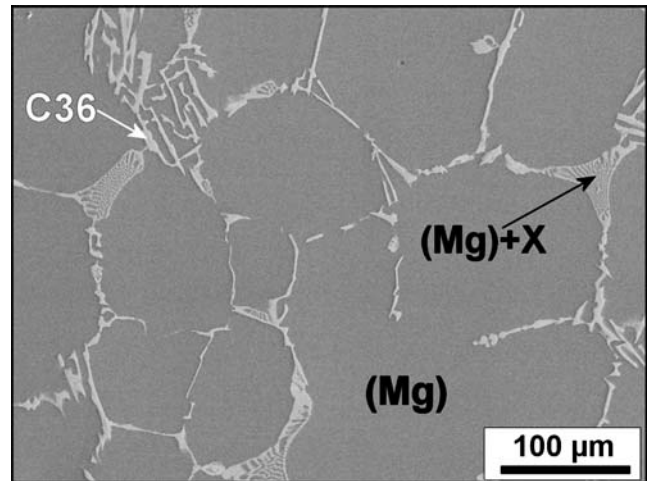


**Fig. 3** Scanning electron micrograph (SEM/BSE) of sample MACS2 after slow cooling in DTA. *X* stands for small amounts of C14 and  $Mg_{17}Sr_2$ , formed in the final eutectic E1 at 508 °C together with (Mg) + C36

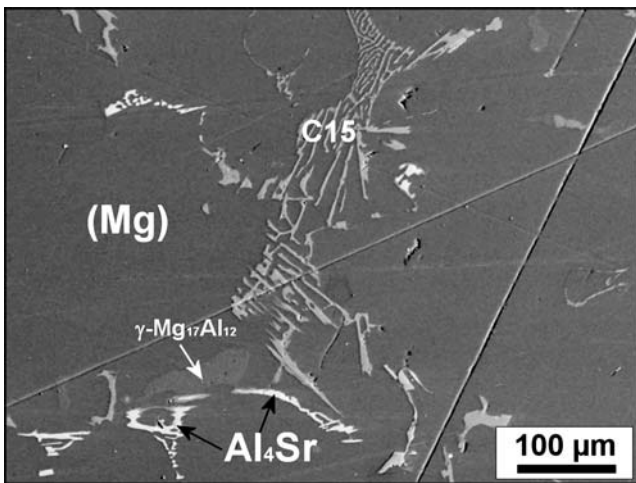


**Fig. 4** Scanning electron micrograph (SEM/BSE) of sample MRI135 after slow cooling in DTA

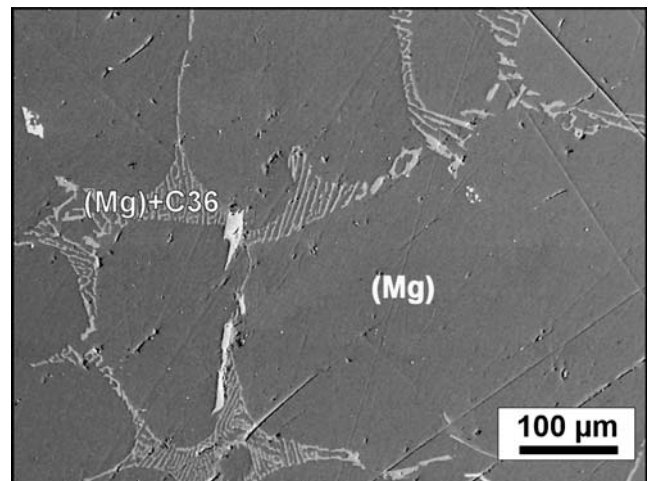


**Fig. 5** Scanning electron micrograph (SEM/BSE) of sample MRI230 after slow cooling in DTA

The microstructure of the quinary commercial alloy sample MRI135 is presented in Fig. 4. As expected from the Mg-rich chemical composition large grains of (Mg) formed. Between these grains areas of finer lamellar microstructures (Mg) + C15 and (Mg) +  $Al_4Sr$  are observed and, in the lower left part of the image, an area of (Mg) +  $\gamma-Mg_{17}Al_{12}$ .

Figure 5 displays the microstructure of sample MRI230. Similar to Fig. 4, the large grains, darkest gray, are (Mg). The fine darkest gray + gray lamellar regions are (Mg) + C36 (probably). As noted previously, it is also possible that this phase is (in total or partly) C15. The chemical analysis of the white particles in the center of the image remained somewhat unclear as not only Al and Mn but also substantial amounts of Mg and Ca as well as some Sr were detected. Most likely these particles are Al-Mn phases and the apparent Mg-Ca-Sr content may be the result of the proximity of nearby C36/C15, possibly present underneath the white particles.

The microstructure of the quinary centroid alloy sample MACSM1 (Fig. 6) looks significantly different compared to the commercial MRI alloys. Large particles with an unusual shape are visible in the left part of the image. Based on the chemical microanalysis with EDX the phase in the center is  $Al_{11}Mn_4$  surrounded peritecticlike by  $Al_4Mn$ . In the top right C15 has grown on  $Al_4Sr$  needles as well as separately only in direct contact with (Mg). A fine microstructure (Mg) +  $Al_4Sr$  exists in the lower part of the figure.

Figure 7 shows the microstructure of sample MACSM2. Small  $Al_8Mn_5$  particles were found in this sample as displayed in the inset on the lower right. The largest precipitates were identified as  $Mg_{17}Sr_2$ , close by C14 is also seen. The remaining matrix is an ultrafine mixture of (Mg) and one or more other phase(s). The inset on the top left shows this matrix structure at higher magnification.

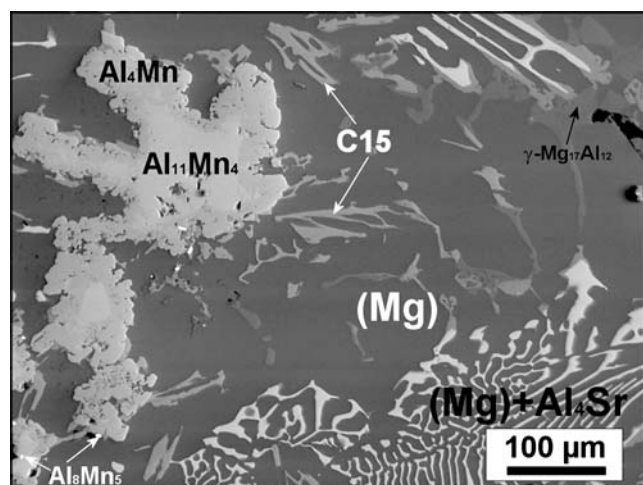


**Fig. 6** Scanning electron micrograph (SEM/BSE) of sample MACSM1 after slow cooling in DTA

The chemical composition of this area averages out to 10 wt.% Ca, 5 to 10 wt.% Sr, small amounts of Al, and balance Mg.

## 4. Thermodynamic Calculations

### 4.1 Thermodynamic Descriptions

The thermodynamic dataset of the four-component system Mg-Al-Ca-Sr comprises the parameters of the four assessed ternary subsystems Mg-Al-Ca,<sup>[11]</sup> Mg-Al-Sr,<sup>[5]</sup> Mg-Ca-Sr, and Al-Ca-Sr (this work, part I<sup>[1]</sup>). No additional quaternary interaction parameter was introduced for the multicomponent calculations.

Within the five-component system Mg-Al-Ca-Sr-Mn five quaternary subsystems, ten ternary subsystems, and ten binary subsystems exist. The prime basis for this system is the quaternary Mg-Al-Ca-Sr system; the database was extended by the four binary subsystems containing Mn and the assessed ternary Mg-Al-Mn system. Tables 4 to 6 list the sources of all binary and ternary subsets of the quinary system except the ternary Ca-Sr-Mn, which is extrapolated. All thermodynamic parameters are given in a publicly available thesis.<sup>[12]</sup>

The important Mg-Al-Mn ternary was recently re-assessed and modeled by Du et al.,<sup>[13]</sup> including and extending the data published previously.<sup>[8]</sup> This is the only thermodynamic description that was changed after the initial calculations were performed to define key samples for the quinary system. Therefore, the results of the final thermodynamic calculations presented here differ somewhat from the initial calculations as discussed later. That is, no parameter adjustment was executed to meet the results of the current experiments; the experimental results were used for comparison or validation only.

It is emphasized that assessed datasets of *all* three Mg-Al-*X* ternaries are included into this five component database, together with the Mg-Ca-Sr and Al-Ca-Sr

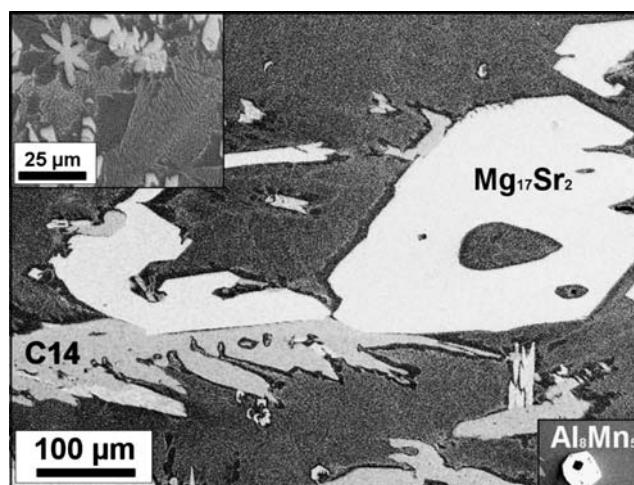


**Fig. 7** Scanning electron micrographs (SEM/BSE) of sample MACSM2 after slow cooling in DTA. The inset at bottom right shows an  $\text{Al}_8\text{Mn}_5$  particle at a different location with same magnification as the main image; the inset at top left shows a higher magnification of the matrix region

ternaries. This covers the interactions among major components. Simple extrapolations comprise ternary systems containing manganese and none or only one of the components Mg and Al. In other words, it is the combination of Mn with Ca or Sr where information is lacking. Since the Al-Mn phases in general exhibit very small solubilities for Ca and Sr, and given the absence of Mg-Mn phases, this limitation is considered acceptable.

### 4.2 Calculated Quaternary Phase Relations

It is not trivial to provide a plain graphical impression of quaternary phase equilibria. A visualization of the main features is attempted by presenting a combination of the liquidus projections of the ternary edge systems of the Mg-Al-Ca-Sr quaternary system in Fig. 8. A tetrahedron comprising quaternary alloy compositions is formed by folding the three Ca-containing ternaries up, thus forming a top vertex at pure Ca. The invariant five phase reactions involving the liquid phase within this tetrahedron are listed in Table 7.

Some of these reactions degenerate almost to a ternary edge system, as discussed previously. For example, the reaction U19 at 445 °C involves a liquid phase composition of only 263 ppm Sr and the transformed  $\text{Al}_4\text{Sr}$  phase fraction is virtually zero (0.000833). The temperature of this reaction is also virtually identical to that of the E2 reaction in the Mg-Al-Ca system.<sup>[11]</sup> Thus, in reality, U19 degenerates to the reaction  $L \leftrightarrow \text{Al}_4\text{Ca} + \beta + \gamma\text{Mg}_{17}\text{Al}_{12}$ .

As pointed out by Kattner<sup>[14]</sup> *true* quaternary phases are generally not to be expected in metallic systems. Quaternary solid phase *compositions* may of course be observed due to solid solutions originating in binary or ternary intermetallic phases. Six examples in the present system are the phases C14 and C15,  $(\text{Ca,Sr})_{0.333}(\text{Al,Mg})_{0.667}$ ,  $\text{Al}_4\text{Ca}$  and  $\text{Al}_4\text{Sr}$ ,  $(\text{Al,Mg})_{0.8}(\text{Ca,Sr})_{0.2}$ , and the phases  $\text{Mg}_{17}\text{Sr}_2$ ,  $(\text{Al,Mg})_{17}(\text{Ca,Sr})_2$ , and  $\text{Mg}_{38}\text{Sr}_9$ ,  $(\text{Al,Mg})_{38}(\text{Ca,Sr})_9$ .



**Table 4 Sources of all ten binary subsystems of the quinary Mg-Al-Ca-Sr-Mn system**

	Mg	Al	Ca	Sr
Al	Liang et al. <sup>[17]</sup>	...	...	...
Ca	Agarwal et al. <sup>[18](a)</sup>	Kevorkov et al. <sup>[19](b)</sup>	...	...
Sr	Zhong et al. <sup>[20]</sup>	Zhong et al. <sup>[21]</sup>	Zhong et al. <sup>[22]</sup>	...
Mn	Gröbner et al. <sup>[23]</sup>	Du et al. <sup>[13]</sup>	Estimation	Estimation

(a) Slightly adjusted in Ref 24:  $G_{Mg:Ca}^{0,C14} = -20,456.3 + 130.6760 * T - 24.04541 * T * \ln(T) - 0.0028942 * T^2 - 2.306 * 10^{-7} * T^3 + 35,456.50 * T^{(-1)}$   
 (b) Slightly adjusted within this work:  $G_{Al:Ca}^{0,C15} = -27,900 + 5 * T + 0.666667 * G_{Al}^{0,fcc} + 0.333333 * G_{Ca}^{0,fcc}$

**Table 5 Sources of the six ternary Mg-X-Y subsystems of the quinary Mg-Al-Ca-Sr-Mn system**

Mg+	Al	Ca	Sr
Ca	Janz et al. <sup>[11]</sup>	...	...
Sr	Janz et al. <sup>[5]</sup>	Janz et al. <sup>[1]</sup>	...
Mn	Du et al. <sup>[13]</sup>	Extrapolation	Extrapolation

**Table 6 Sources of the three ternary Mg-free Al-X-Y subsystems of the quinary Mg-Al-Ca-Sr-Mn system**

Al+	Ca	Sr
Sr	Janz et al. <sup>[1]</sup>	...
Mn	Extrapolation	Extrapolation

Because of this abundance of phases that may appear “quaternary” in a microstructure analysis, it is quite difficult to definitely exclude the existence of true quaternary phases. This restriction is made because of the fine eutectic structure, denoted as (Mg) + X in Fig. 3 and discussed in Section 5.1.

The combination of the ternary liquidus surfaces in Fig. 8 provides an overview of the primary precipitates expected in the quaternary system. All these solid phases do have their origin in the binary or ternary subsystems. However, solid solution ranges may extend into quaternary compositions, without defining a separate quaternary phase. For example, the C14 Laves phase exists in a complete solid solution between Mg<sub>2</sub>Ca and Mg<sub>2</sub>Sr, but also dissolves some aluminum. This is reflected in the thermodynamic sublattice model (Al,Mg)<sub>2</sub>(Ca,Sr), where the bold Mg denotes a majority constituent on the first sublattice. Accordingly, the three individual primary precipitation areas of C14 in the edge systems merge to a single primary precipitation volume of C14 in the quaternary composition tetrahedron. The entire tetrahedron is filled by such volumes extending from the edge systems in Fig. 8.

A nearly symmetric volume is spanned in the Mg corner where (Mg) is the primary phase. This field is in contact with six other fields of primary precipitation. Additions of Ca to Mg cause a primary precipitation of C14-Mg<sub>2</sub>Ca while additions of Sr lead to primary precipitation of Mg<sub>17</sub>Sr<sub>2</sub>. Additions of Al and Ca or Sr form Al<sub>4</sub>Sr, τ, and γ. The primary fields of τ, Al<sub>38</sub>Mg<sub>58</sub>Sr<sub>4</sub>, and γ, Mg<sub>17</sub>Al<sub>12</sub>, are

**Table 7 All 24 invariant five-phase reactions involving liquid phase in the quaternary Mg-Al-Ca-Sr system**

Type	T/°C, calculated	Reaction	T/°C, experimental
U1	697	L + Al <sub>2</sub> Sr + C15 ↔ Al <sub>4</sub> Sr + C14	...
U2	610	L + Al <sub>2</sub> Sr + Mg <sub>23</sub> Sr <sub>6</sub> ↔ C14 + Mg <sub>38</sub> Sr <sub>9</sub>	...
U3	586.4	L + Al <sub>2</sub> Sr + Mg <sub>38</sub> Sr <sub>9</sub> ↔ Mg <sub>17</sub> Sr <sub>2</sub> + C14	...
U4	585.6	L + Al <sub>2</sub> Sr ↔ Al <sub>4</sub> Sr + Mg <sub>17</sub> Sr <sub>2</sub> + C14	...
U5	561	L + Al <sub>4</sub> Sr + C14 ↔ C15 + Mg <sub>17</sub> Sr <sub>2</sub>	...
U6	544	L + C15 + C14 ↔ Mg <sub>17</sub> Sr <sub>2</sub> + C36	...
U7	512	L + C36 ↔ Mg <sub>17</sub> Sr <sub>2</sub> + (Mg) + C15	...
E1	508	L ↔ Mg <sub>17</sub> Sr <sub>2</sub> + C14 + C36 + (Mg)	508
U8	505	L + Mg <sub>17</sub> Sr <sub>2</sub> ↔ C15 + (Mg) + Al <sub>4</sub> Sr	505
U9	475	L + Al <sub>4</sub> Sr + C36 ↔ cMg <sub>17</sub> Al <sub>12</sub> + C15	...
U10	474	L + Al <sub>2</sub> Sr + C15 ↔ C14 + Al <sub>7</sub> Sr <sub>8</sub>	...
U11	473	L + C15 ↔ Al <sub>4</sub> Sr + Al <sub>4</sub> Ca + γMg <sub>17</sub> Al <sub>12</sub>	...
U12	468	L + Al <sub>4</sub> Sr + C36 ↔ C15 + τAlMgSr	...
U13	467.4	L + Al <sub>4</sub> Sr ↔ C36 + τAlMgSr + γMg <sub>17</sub> Al <sub>12</sub>	...
U14	466.8	L + Al <sub>4</sub> Sr ↔ C15 + τAlMgSr + (Mg)	...
U15	465	L + C15 ↔ C36 + τAlMgSr + (Mg)	...
U16	462	L + Al <sub>3</sub> Sr <sub>8</sub> + Al <sub>2</sub> Sr ↔ C14 + Al <sub>7</sub> Sr <sub>8</sub>	...
U17	454	L + C36 ↔ sAlMgSr + (Mg) + γMg <sub>17</sub> Al <sub>12</sub>	...
U18	446	L + Al <sub>4</sub> Sr ↔ (Al) + Al <sub>4</sub> Ca + β	...
U19	445	Al <sub>4</sub> Sr + L ↔ Al <sub>4</sub> Ca + β + γMg <sub>17</sub> Al <sub>12</sub>	...
U20	380	L + Al <sub>3</sub> Sr <sub>8</sub> ↔ C14 + Al <sub>7</sub> Sr <sub>8</sub> + (Al)	...
U21	330	L + C15 + AlCa ↔ Al <sub>7</sub> Sr <sub>8</sub> + Al <sub>3</sub> Ca <sub>8</sub>	...
U22	318	L + C15 ↔ C14 + Al <sub>7</sub> Sr <sub>8</sub> + Al <sub>3</sub> Ca <sub>8</sub>	...
E2	228	L ↔ C14 + Al <sub>7</sub> Sr <sub>8</sub> + Al <sub>3</sub> Ca <sub>8</sub> + αSr	...

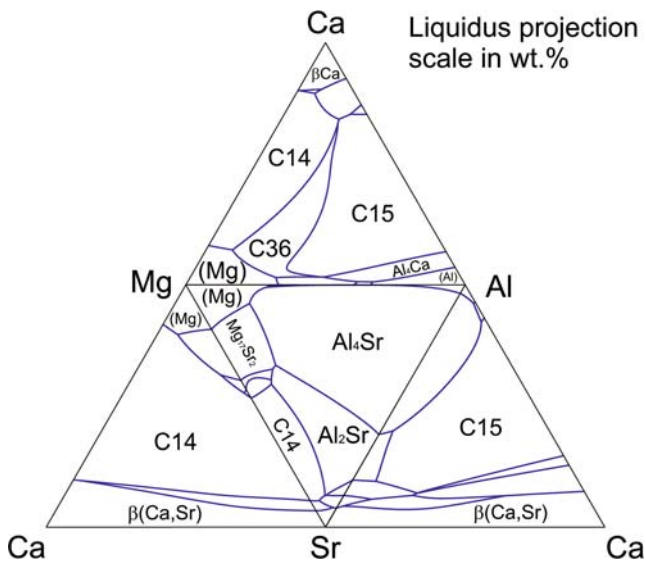
too small to be labeled in Fig. 8. The C36 phase forms the primary precipitate by adding a combination of Al and an increased amount of Ca.

Figure 9 is constructed in the same way as Fig. 8 by joining the four ternary isothermal sections at 700 °C. It highlights the significant existence of the liquid phase extending from pure Mg into a wide composition range. At 700 °C, six solid phases are in equilibrium with this

## Section I: Basic and Applied Research

liquid: C14, C36, C15, Al<sub>4</sub>Sr, Al<sub>2</sub>Sr, and the distant β-(Ca,Sr) is touched as seen best in the almost completely molten Mg-Ca-Sr system.

The corresponding phase diagram at 500 °C is shown in Fig. 10. At this temperature only four solid phases are in equilibrium with the emerged solid (Mg) phase: Al<sub>4</sub>Sr, Mg<sub>17</sub>Sr<sub>2</sub>, and C14-Mg<sub>2</sub>(Ca,Sr) starting from the corresponding binary edges, and the ternary C36, which is located in the Mg-Al-Ca system. These phases are labeled in the diagram with the numbers given in the legend. It is



**Fig. 8** Combination of the calculated ternary liquidus projections from the four subsystems of the Mg-Al-Ca-Sr quaternary system. A tetrahedron comprising quaternary alloy compositions is formed by folding the three Ca-containing ternaries up, thus forming a vertex with pure Ca on top

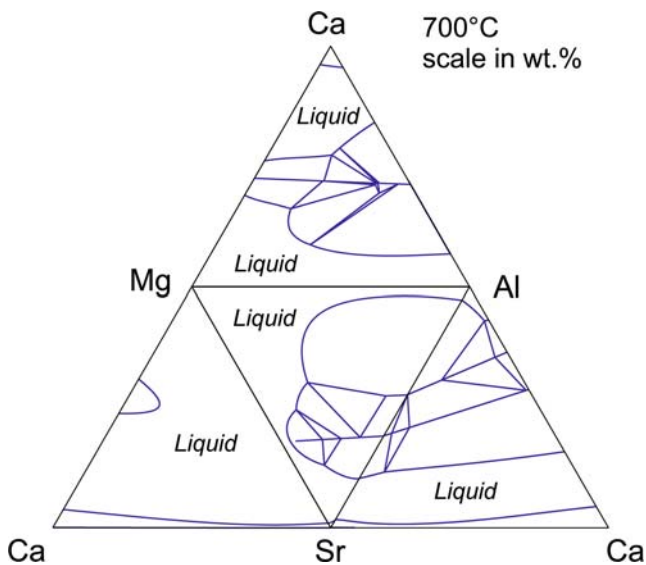


**Fig. 9** Combination of the calculated ternary isothermal sections at 700 °C from the four subsystems of the Mg-Al-Ca-Sr quaternary system

noteworthy that a Mg-Al-rich liquid (marked with *L*) still exists at this temperature and is in contact with the (Mg) phase field. Further residual liquid areas, close to the Ca corner and close to each Ca-Sr binary, merge to the second liquid volume in the quaternary tetrahedron.

The phase labeling in the next isothermal diagram at 400 °C (Fig. 11) is consistent with Fig. 10. At 400 °C the C36 phase, which is No. 4 at 500 °C, is no longer stable. Its equilibrium with the (Mg) phase is taken over by the C15 phase (No. 5). The Mg-Al-rich liquid is solidified at this

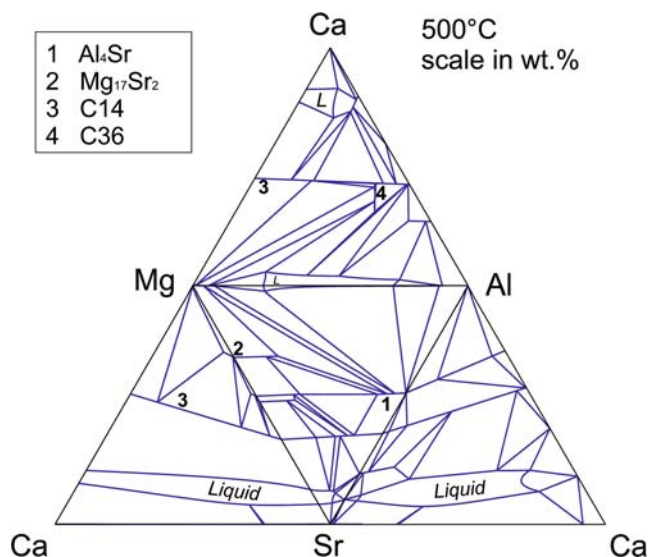


**Fig. 10** Combination of the calculated ternary isothermal sections at 500 °C from the subsystems of the Mg-Al-Ca-Sr quaternary system. Solid phases in equilibrium with (Mg) are labeled with numbers

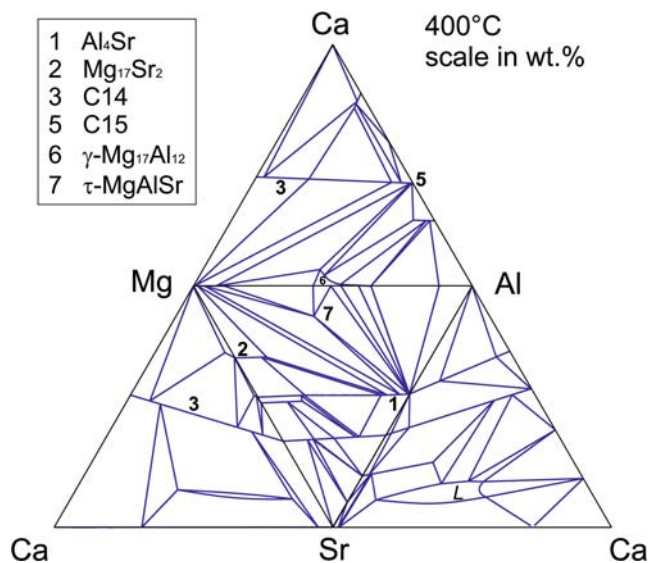


**Fig. 11** Combination of the calculated ternary isothermal sections at 400 °C from the subsystems of the Mg-Al-Ca-Sr quaternary system. Labeling of solid phases in equilibrium with (Mg) is consistent with Fig. 10

lower temperature and brought forward two additional phases in equilibrium with (Mg): On the Ca side  $\gamma\text{Mg}_{17}\text{Al}_{12}$  (with Ca dissolved, No. 6) and on the Sr side the ternary phase  $\tau\text{-AlMgSr}$  with stoichiometry  $\text{Al}_{38}\text{Mg}_{58}\text{Sr}_4$  (No. 7).

### 4.3 Calculated Quinary Phase Relations

Visualization of the calculated Mg-Al-Ca-Sr-Mn phase relations is attempted in analogy to the figures presented previously for the quaternary system: projections of the ternary liquidus surfaces, and ternary isothermal sections are combined in the following diagrams. All diagrams are constructed with the same arrangement of the ternary systems. In the center of each diagram the triangular-shaped quaternary diagram of the core system Mg-Al-Ca-Sr from Fig. 8 to 11 is found; the additional six subsystems containing Mn are added to the left and right. Duplications of ternary systems do not occur in these “quinary” Fig. 12 to 15. The total is ten ternary systems, with the four Mn-free core ternaries and six additional Mn-X-Y ternaries. The only additionally assessed system, Mg-Al-Mn, can be found top right; the remaining five are calculated by extrapolation. In these diagrams the cut-and-fold approach to visualize a quaternary tetrahedron only works for Mg-Al-Ca-Sr; this is

because of the arrangement of all ten ternary edge systems without duplication. To visualize, for example, the Mg-Al-Ca-Mn quaternary tetrahedron requires rearrangement of two ternaries.

In the combination of the projected liquidus surfaces, Fig. 12, the extended liquid miscibility gaps stand out in all six Mn-containing ternary systems, especially striking in the Al-free ones. These miscibility gaps are already present in the three Mn-(Mg,Ca,Sr) binary systems and extend to the ternary. Since no assessment is available for five of these ternary systems, marked by “E” in the diagram, the size of the miscibility gaps may be over- or underestimated by the extrapolation. The fields of primary (Mg) are very small in the ternaries with Mn in contrast to the Mg-Al-Ca-Sr system. In total, 46 invariant six-phase reactions involving the liquid phase were identified in the quaternary Mg-Al-Ca-Sr-Mn system. Only 12 involve the (Mg) phase as a reactant, and those six that are not degenerate to the already known quaternary Mg-Al-Ca-Sr are listed in Table 8. None of these show a eutectic reaction type. The only eutectic found in the quinary at all is  $L \leftrightarrow \text{Mg}_{17}\text{Sr}_2 + \text{C14} + \text{C36} + (\text{Mg}) + \text{Al}_8\text{Mn}_5$ ; however, it is degenerate, only 0.01 K below the eutectic E1 at 508 °C given in Table 7, with negligible fraction of  $\text{Al}_8\text{Mn}_5$ .

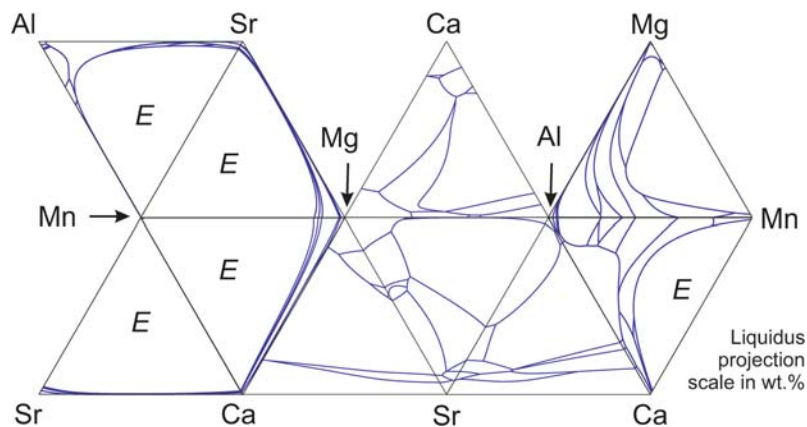


**Fig. 12** Combination of the calculated ternary liquidus projections for all ten subsystems of the Mg-Al-Ca-Sr-Mn quinary system. The five systems denoted by ‘E’ are calculated as extrapolation from the binary data, all other systems are assessed

**Table 8** Invariant six-phase reactions in the quinary Mg-Al-Ca-Sr-Mn system involving the liquid and the (Mg) phase; six more reactions are excluded from this table since they are degenerate to the quaternary Mg-Al-Ca-Sr system

Type	T/°C, calculated	Reaction	T/°C, experimental
5cU13	511.3	$L + \text{Al}_8\text{Mn}_5 \leftrightarrow \text{C14} + \text{Mg}_{17}\text{Sr}_2 + \beta\text{Mn} + (\text{Mg})$	(a)
5cU14	510.9	$L + \beta\text{Mn} + \alpha\text{Mn} \leftrightarrow \text{C14} + \text{Mg}_{17}\text{Sr}_2 + (\text{Mg})$	...
5cU19	492	$L + \text{C36} + \text{Al}_8\text{Mn}_5 \leftrightarrow (\text{Mg}) + \text{C15} + \text{Al}_{11}\text{Mn}_4$	...
<b>5cU20</b>	490	$L + \text{Al}_8\text{Mn}_5 \leftrightarrow (\text{Mg}) + \text{C15} + \text{Al}_4\text{Sr} + \text{Al}_{11}\text{Mn}_4$	490
5cU26	467.9	$L + \text{Al}_{11}\text{Mn}_4 + \text{C36} \leftrightarrow (\text{Mg}) + \text{C15} + \text{Al}_4\text{Mn}$	...
5cU27	467.7	$L + \text{Al}_{11}\text{Mn}_4 \leftrightarrow (\text{Mg}) + \text{C15} + \text{Al}_4\text{Sr} + \text{Al}_4\text{Mn}$	...

(a) Aimed at with sample MACSM2, but shifted off that composition due to the later Mg-Al-Mn description

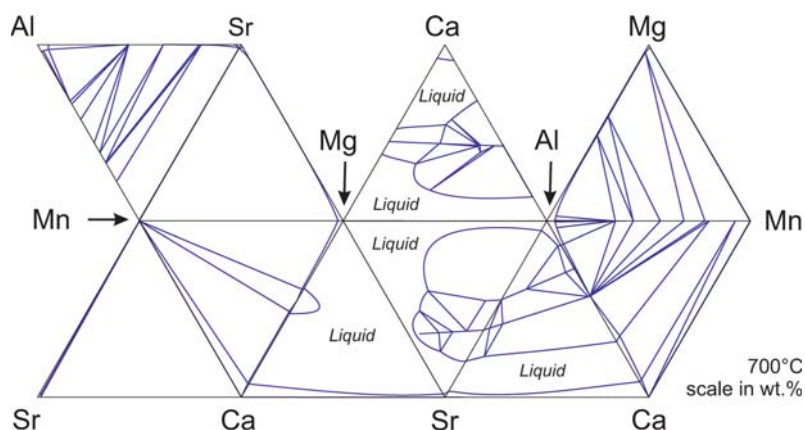


**Fig. 13** Combination of the calculated ternary isothermal sections at 700 °C from the subsystems of the Mg-Al-Ca-Sr-Mn quinary system

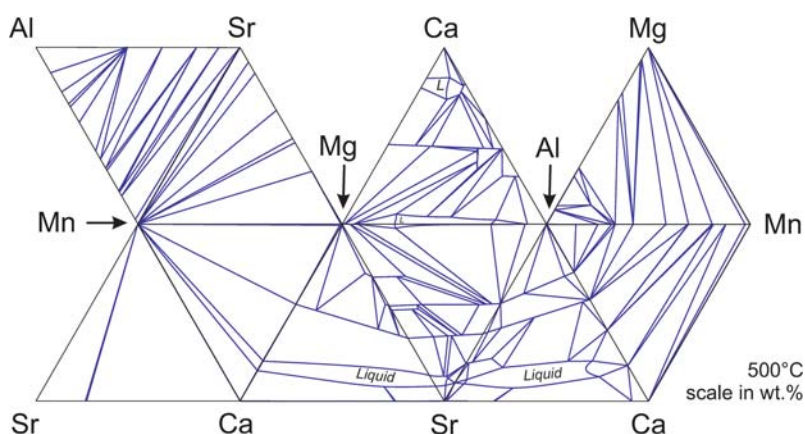


**Fig. 14** Combination of the calculated ternary isothermal sections at 500 °C from the subsystems of the Mg-Al-Ca-Sr-Mn quinary system

The combination of the isothermal sections at 700 °C is presented in Fig. 13. The Mg-Al-Ca-Sr system is present in the center of the diagram showing large liquid regions. Most of the additional Mn-induced phase equilibria are either toward the pure  $\alpha$ Mn or toward the binary Al-Mn phases, which also have high melting points. In application to melting technology of Mg alloys it is evident that for complete melting at 700 °C large composition ranges are available for alloying elements Al, Ca, and Sr, but not for Mn.

More intricate phase relations evolve at 500 °C (Fig. 14). The (Mg) solid solution range essentially exists along the Mg-Al binary with minute amounts of Ca, Sr, and Mn. Most of the binary intermetallic phases are already stable and form various equilibria. The liquid phase essentially exists only in the same two smaller regions already detailed for the quaternary Mn-free system with very small Mn solubility. Most important is the Mg-Al rich liquid range.

Figure 15 displays the combination of the ternary isothermal sections at 400 °C. Only two liquid areas exist, one in the Mg-Ca-Sr system and one in the Al-Ca-Sr system close to the Ca-Sr binary edge, which is the same as in Fig. 11. The (Mg) solid solution is not in equilibrium with

any liquid phase. The disappearing C36 phase and the occurrence of  $\tau$ -AlMgSr phase, which is present in the Mg-Al-Sr system close to the Mg-Al binary edge, is the same as in the Mn-free system. In the Mg-Ca-Mn system, two predominant three-phase areas exist:  $\alpha$ Mn + C14 + (Mg) and  $\alpha$ Mn + C14 +  $\alpha$ Ca. No phase boundary is visible in the Ca-Sr-Mn system; a two phase region  $\alpha$ Mn +  $\alpha$ (Ca,Sr) covers the entire range of the phase diagram. This is due to the complete solubility between Ca and Sr at 400 °C and the vanishing mutual solubility with Mn.

## 5. Comparison between Experimental Data and Calculations

### 5.1 Quaternary Alloys

Looking at the DTA results given in Table 3, it is noted that the calculated transition temperatures at 522 and 504 °C for sample MACS1 were not experimentally observed. This is consistent with the expected signal strength predicted by the calculation, which is demonstrated by the calculated

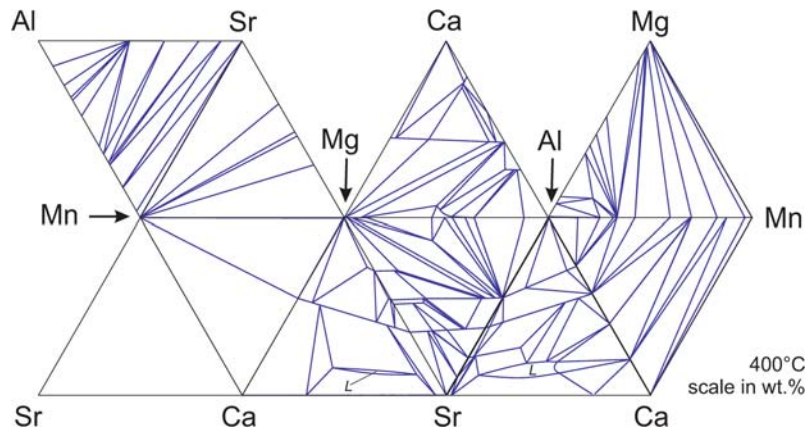


**Fig. 15** Combination of the calculated ternary isothermal sections at 400 °C from the subsystems of the Mg-Al-Ca-Sr-Mn quinary system

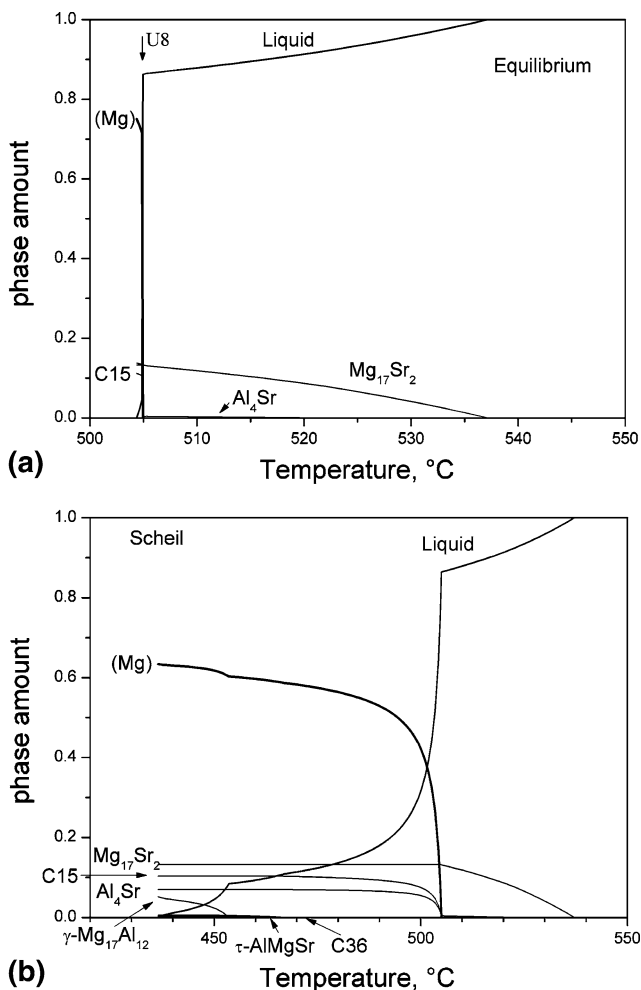


**Fig. 16** Calculated solidification under different cooling conditions for the composition of sample MACS1. (a) Equilibrium conditions; (b) Scheil conditions

amounts of all phases during equilibrium cooling of sample MACS1 in Fig. 16(a) and for the solidification under Scheil conditions in Fig. 16(b). It is obvious from Fig. 16(a) why

only two significant thermal signals could have been detected with DTA: The first one corresponds to the primary precipitation of  $Mg_{17}Sr_2$  at 537 °C, the second one to the abrupt solidification of about 80% of the sample while passing the U8 transformation reaction at 505 °C under equilibrium conditions. Under Scheil conditions the reaction U8,  $L + Mg_{17}Sr_2 \leftrightarrow C15 + (Mg) + Al_4Sr$  cannot occur. Even though at exactly the same temperature of 505 °C the drastic drop of liquid phase amount due to the starting crystallization of mostly (Mg) with some  $C15 + Al_4Sr$ , shown in Fig. 16(b), should produce a very strong signal. These expected signals, under both equilibrium and Scheil conditions, are perfectly consistent with the DTA results. The other phase transformations calculated for sample MACS1 at 522 and 504 °C involve indiscernible bends in the fraction liquid curve and are impossible to detect with thermal analysis.

The microstructure of this sample, presented in Fig. 2, is also in reasonable agreement with the thermodynamic calculations. All phases covered by the calculation under equilibrium conditions are present in the sample. The relative phase amounts observed in the microstructure indicate that the solidification may have followed the Scheil conditions more closely. The phase sequence is also in essence consistent with the calculation. The coarse  $Mg_{17}Sr_2$  particles are in accord with the primary crystallization mode and the finer structures of  $(Mg) + C15 + Al_4Sr$  with the precipitation reaction at/below U8. The occasionally found larger grain size of C15 is not consistent; these blocky particles might have formed during the sample preparation and never actually remelted.

For sample MACS2 the liquidus temperature and the significant amount of primary (Mg) is validated and also the secondary C36 precipitation, jointly with (Mg) as demonstrated in Fig. 3. The calculation also predicted small amounts of C14 and  $Mg_{17}Sr_2$ , formed in the final eutectic E1 at 508 °C together with (Mg) + C36. The eutectic molar phase fractions are 0.62 (Mg), 0.18 C14, 0.13  $Mg_{17}Sr_2$ , and 0.07 C36, respectively. The eutectic structure and especially the eutectic temperature are in perfect agreement with the calculation. The eutectic minority phases could not be identified in the microstructure given in Fig. 3 and denoted

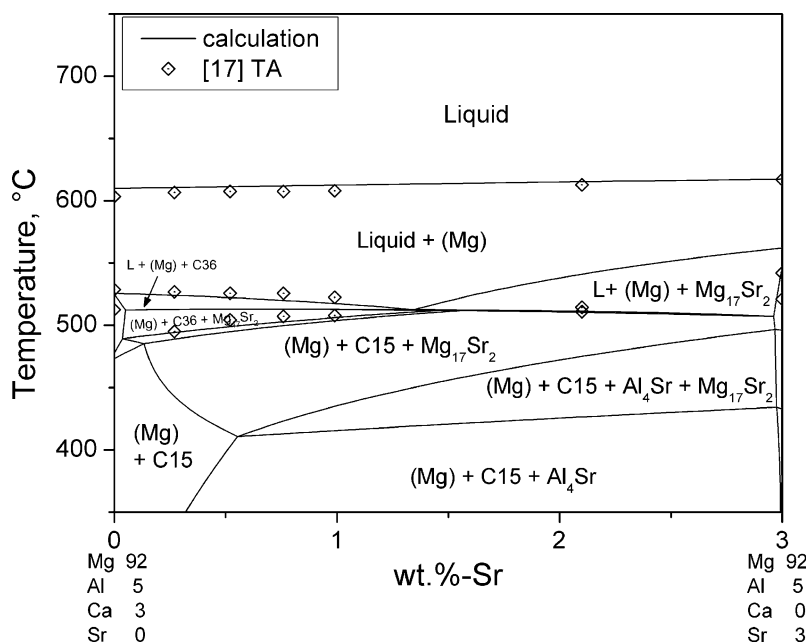


**Fig. 17** Calculated quaternary vertical phase diagram section from  $\text{Mg}_{92}\text{-Al}_5\text{-Ca}_3$  to  $\text{Mg}_{92}\text{-Al}_5\text{-Sr}_3$  (wt.%). The thermal analysis data of Suzuki et al.<sup>[17]</sup> are superimposed

as “X.” All three of these intermetallic solid solution phases, C14,  $\text{Mg}_{17}\text{Sr}_2$ , and C36, may exhibit quaternary compositions as detailed in Section 4.2. The similar average atomic mass of these phases will give only a poor contrast in the BSE image, making the distinction within the fine microstructure impossible.

The results published by Suzuki et al.<sup>[15]</sup> from thermal analysis during cooling in a steel crucible (0.6 K/s) are compared with the phase diagram section calculated in the present work in Fig. 17. This section shows the phase boundaries at constant 92 wt.% Mg and 5 wt.% Al with an exchange of Ca by Sr, that is for a composition range  $\text{Mg}_{92}\text{-Al}_5\text{-Ca}_3$  to  $\text{Mg}_{92}\text{-Al}_5\text{-Sr}_3$  (wt.%). The thermal signals of the six virtually manganese-free samples are well reproduced by the thermodynamic calculation. (Mg) is the primary precipitate in all these alloys. The secondary phase is either C36 for the Ca-rich alloys or  $\text{Mg}_{17}\text{Sr}_2$  for those with more Sr than Ca. These calculated results agree with the experimentally found microstructures<sup>[15]</sup> in addition to the thermal signals.

At lower temperatures and up to 0.5 wt.% Sr only (Mg) and C15 are calculated to be stable; some additional  $\text{Al}_4\text{Sr}$  may form at higher Sr content. In the Sr-free sample the C14 phase was detected,<sup>[15]</sup> which is also reproduced by the thermodynamic calculations assuming Scheil conditions for the solidification. This scenario is acceptable since the cooling rate used in these TA experiments is 36 K/min and thus much higher than the 1 to 5 K/min used in DTA of this work.

## 5.2 Quinary Alloys

The thermal signals obtained for the various five-component samples by DTA are compared with the calculated equilibrium solidification phase boundaries of

each sample in Table 2. It is obvious that a number of experimental signals are missing compared to the calculation. This may well be explained by more detailed calculations, also showing the converted phase amounts, as demonstrated in the following, starting with the commercial MRI alloys.

The primary precipitation of the Al-Mn phases, especially of  $\text{Al}_8\text{Mn}_5$ , is usually not detected by DTA in Mg alloys as discussed by Ohno et al.,<sup>[4]</sup> because the evolved phase amount of these phases is too small. This is also observed here. Many other reactions in the calculated solidification paths also produce only small additional phase amounts. This is shown in more detail for sample MRI135 in Fig. 18, comparing the results of the solidification under equilibrium conditions (Fig. 18a) to those of the solidification under Scheil conditions (Fig. 18b). Note that a logarithmic scale was selected to resolve the minority phase amounts. Magnesium alloys typically solidify along a path somewhere in between these two extreme models as discussed in Ohno et al.,<sup>[4]</sup> also depending on the Al content. The MRI135 alloy confirms this typical feature: the  $\gamma\text{Mg}_{17}\text{Al}_{12}$  phase forms a substantial amount of about 7% below 454 °C under Scheil conditions in contrast to the equilibrium solidification. This phase was in fact detected in small amounts in the microstructure, Fig. 4. Moreover, the strongest observed “Liquidus” signal is in perfect agreement with the massive solidification of (Mg) under both models. The next major bend in the  $f^{\text{Liquid}}(T)$  curve, caused by the C15 precipitation, is also very close to the experimental value of 506 °C, compared with the equilibrium calculation at 503 °C.

A vertical phase diagram section representing both MRI samples is presented in Fig. 19. The Mn and Sr contents are

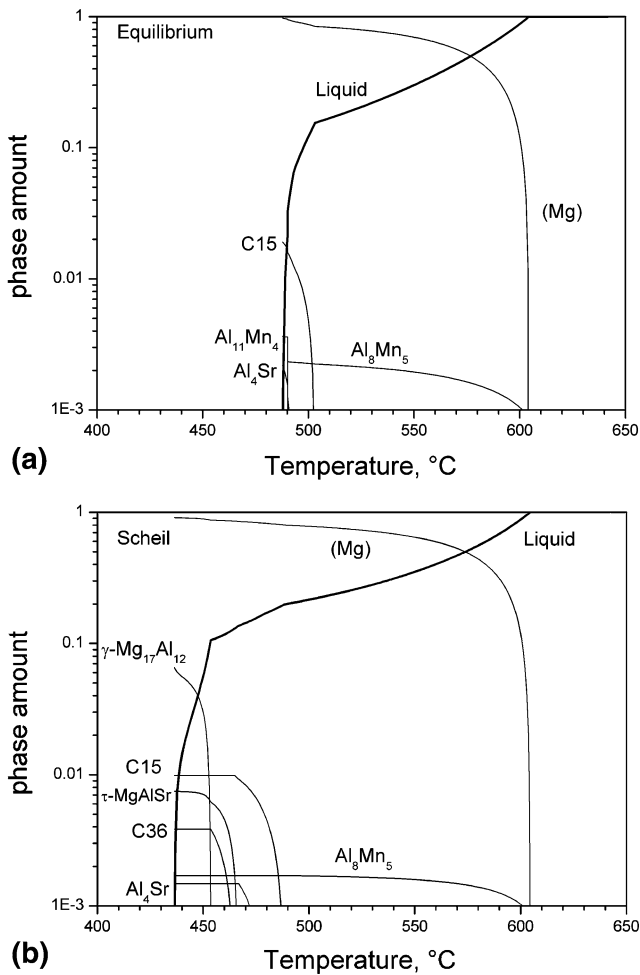


**Fig. 18** Calculated solidification under different cooling conditions for the composition of sample MRI135: (a) Equilibrium conditions; (b) Scheil conditions

fixed for the whole diagram range while Al and Ca are varied to meet the two sample compositions; Mg is selected as balance. The thermal signals from our DTA experiments for both samples are in nice agreement with the calculation and correlate with the start of massive solidification of the two majority phases in each sample, (Mg) and C15/C36. This is also demonstrated by the  $f^\phi$  calculation of Fig. 18. The lacking signal of the true primary phase  $\text{Al}_8\text{Mn}_5$  is also consistent with the calculation; only trace amounts precipitate above the majority solidification of (Mg), even below the cut-off limit of  $f^\phi = 0.001$  in these diagrams.

Figure 20 shows the vertical phase diagram section constructed to meet the composition of the two quinary key samples. This section covers a composition range starting from an almost ternary Mg-Ca-Sr alloy and ending at an almost ternary Mg-Al-Mn alloy, as marked on the abscissa.

The first synthetic alloy, MACSM1, was selected at the centroid composition of the key invariant reaction 5cU20, calculated at 490 °C. The composition range of this reaction is actually a polyhedron volume within the five-dimensional

composition space of the Mg-Al-Ca-Sr-Mn system. A one-dimensional line is cut out of that polyhedron volume by the series of alloys defining the phase diagram section. This cutout is a composition range of reaction 5cU20, which is highlighted in Fig. 20 by the bold line. The predicted temperature of this reaction is exactly confirmed by this sample. The relevance of the centroid alloy sample concept is emphasized by comparison to sample MRI135, which should also pass this reaction, but no signal was detected, as given in Table 2.

The reason is that the phase amounts converted in this reaction is too small in sample MRI135. As visualized in the schematic Fig. 1, the composition of sample MRI135 is indeed within the area of the reaction, but somewhere far from the centroid, while the composition of sample MACSM1 is right at the position of alloy 2, where the complete reaction occurs. This direct hit into the centroid point of a polyhedron volume within the five-dimensional composition space was only possible using the selection algorithm presented in Section 2.

Even though this invariant reaction 5cU20 was identified as one of the most relevant ones for quinary interactions in Mg-rich alloys, its centroid composition, defining the key sample MACSM1, is far from the Mg corner. The composition with less than 50 wt.% Mg but more than 30 wt.% Al, and almost 16 wt.% Mn is therefore quite unusual for Mg-based alloys, however optimized for this validation purpose. As expected from the calculated equilibrium solidification (Fig. 21), substantial amounts of Al-Mn phases were detected in the microstructure (Fig. 6). The major equilibrium phases (Mg),  $\text{Al}_{11}\text{Mn}_4$ , C15, and  $\text{Al}_4\text{Sr}$  are all present in the microstructure.

The primary phase  $\text{Al}_8\text{Mn}_5$  essentially transforms to  $\text{Al}_{11}\text{Mn}_4$ , appearing in the form of the large primary particles. This transformation, essentially during the transition type reaction, may not completely attain equilibrium, thus retaining some  $\text{Al}_8\text{Mn}_5$  and nonequilibrium  $\text{Al}_4\text{Mn}$ . The small amounts of  $\gamma\text{Mg}_{17}\text{Al}_{12}$  detected in the microstructure start in fact forming under Scheil conditions at 454 °C, which is close to the temperature of 463 °C detected with DTA but not assigned in the equilibrium column in Table 2.

The microstructure of sample MACSM2 (Fig. 7) is in reasonable agreement with the calculation. Small primary  $\text{Al}_8\text{Mn}_5$  particles were found in the sample and the major phases are (Mg) together with C14 and  $\text{Mg}_{17}\text{Sr}_2$ . Several thermal signals were detected within a narrow temperature range, which made a proper separation almost impossible, even at 1 K/min heating/cooling rate. The calculated temperatures of the precipitation start of  $\text{Mg}_{17}\text{Sr}_2$  fit exactly the thermal signals. The following three calculated reactions appear very close to each other within a temperature interval of only 0.6 K. Although the final reaction during the solidification of this sample is not calculated as “invariant,” the remaining 90% of the liquid phase is expected to solidify within a narrow temperature interval of only 0.05 K, see Fig. 22. These jammed reactions may explain both the ultrafine microstructure and the very strong thermal signal, even though this is observed at 505 °C, about 6 to 7 K below the calculated main solidification. The initially

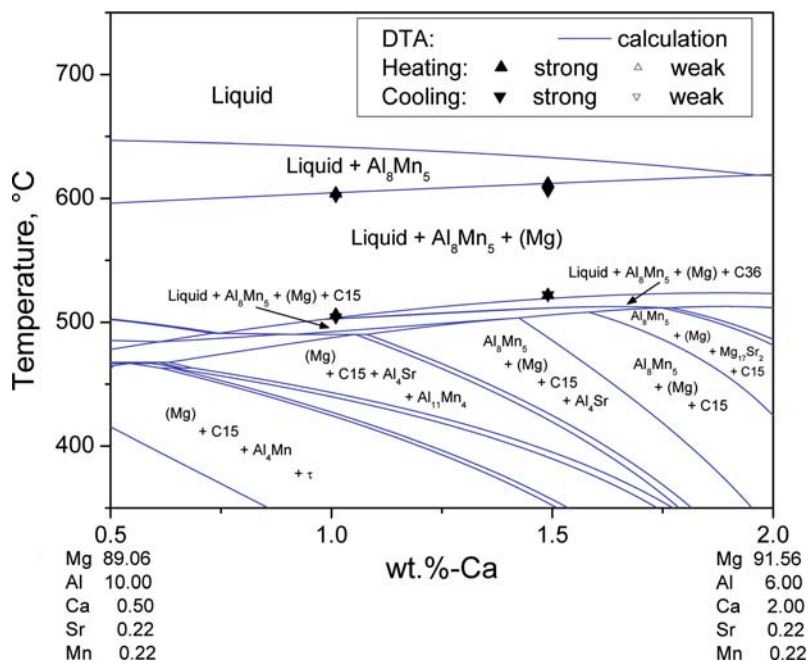


**Fig. 19** Calculated vertical phase diagram section in the Mg-Al-Ca-Sr-Mn quinary system compared with experimental data from DTA for samples MRI135 (at 1.01 wt.% Ca) and MRI230 (at 1.49 wt.% Ca)

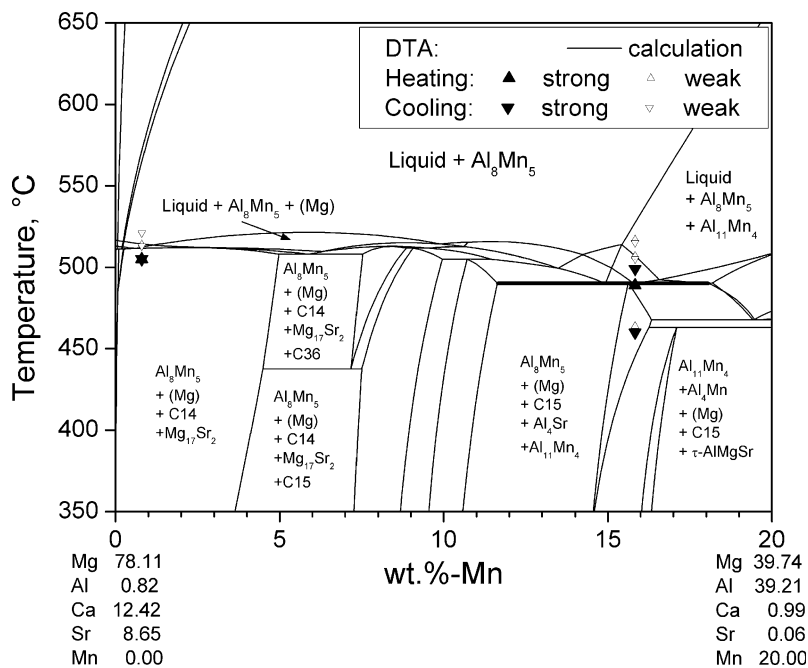


**Fig. 20** Calculated vertical phase diagram section in the Mg-Al-Ca-Sr-Mn quinary system compared with experimental data from DTA for samples MACSM1 and MACSM2. The bold line between 11.6 and 18.2 wt.% Mn indicates the cut-out of the invariant reaction 5cU20 at 490 °C

calculated invariant reaction, aimed at with this sample composition, does not appear in this final calculated phase diagram section because of the two different Mg-Al-Mn ternary datasets used for the key samples selection<sup>[8]</sup> and the later interpretation.<sup>[13]</sup>

## 6. Impact of Ternary Assessed Systems

A reliable calculation of multicomponent phase diagrams requires at least the thermodynamic descriptions of the



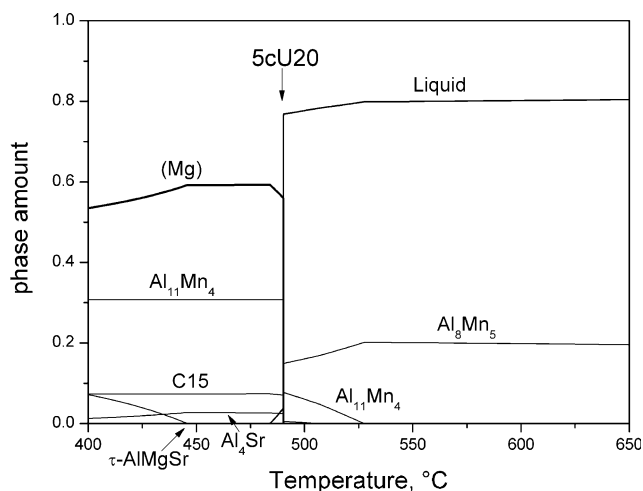


**Fig. 21** Calculated equilibrium phase amounts during solidification of sample MACSM1

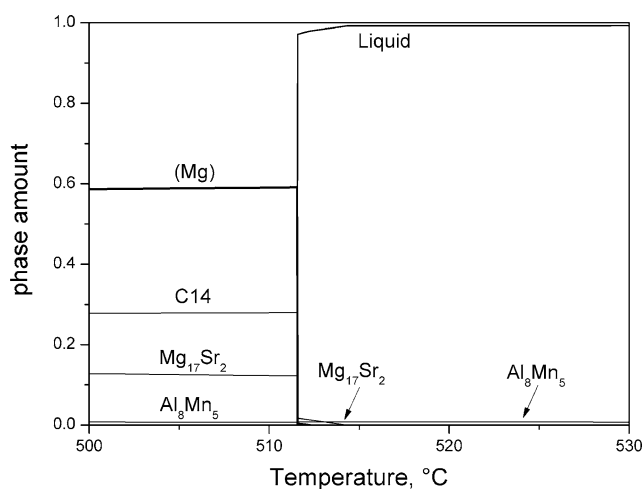


**Fig. 22** Calculated equilibrium phase amounts during solidification of sample MACSM2

binary subsystems. It is assumed in the Calphad community that the relevant ternary subsystems are also important. However, how large is the difference if one sets all the ternary interactions and phase diagram data aside and assumes that a careful description of the binary systems is enough? Also, what about using less elaborate ternary data? The answer will depend on the specific alloy system, but may be quantitatively exemplified at this point for the quinary system Mg-Al-Ca-Sr-Mn by a comparison of four different thermodynamic data sets, D1 to D4:

- D1: Current description, given in Table 4 to 6.
- D2: As D1, but different set for the Mg-Al-Ca system, that considers only the experimental data in the Mg-rich corner of this ternary.<sup>[10]</sup>
- D3: As D1, but an earlier data set for the Mg-Al-Ca system, that includes neither the C36 phase nor the recent experimental data in the Mg-rich corner.<sup>[16]</sup>

D4: Using all of the binary parameter sets of D1, but neglecting all ternary interactions, ternary phases and solubilities in binary compounds. Just the binary  $Mg_2Ca$  and  $Mg_2Sr$  phases are unified to form a single-phase C14 with ideal solution, since they crystallize in the same structure. If no mutual solubility of  $Mg_2Ca$  and  $Mg_2Sr$  are assumed in the C14 phase the results are even worse compared to the D4 option.

In a first step the results based on the most similar data sets D2 and D1 are compared. Only in that case are calculated phase boundaries and reactions at least qualitatively the same for the selected alloy compositions of Table 2 and 3. However, the temperatures differ, for example at the invariant reactions U8: 509 °C (505), E1: 509 °C (508), 5cU20: 496 °C (490); (values for D1 given in brackets). These differences (except for E1) are significant, given the facts that the experimental data validate the D1 results exactly and that the overall uncertainty of DTA measurements for temperature determination is estimated as  $\pm 2$  K for the strong and clear signals of the invariant reactions.

The comparison of results from D3 and D1 shows not only a larger-temperature variation, more importantly the types of phases and the reactions change, thus hampering the assignment of temperatures to phase boundaries. This concerns not only the missing C36 phase in D3, but many other phase boundaries as well. For example, the invariant reactions E1, sample MACS2, and 5cU20, sample MACSM1, no longer exist as *invariant* reactions in the calculations with D3; one may only observe some boundaries of open-phase fields around these temperatures.

This problem is further worsened when comparing the results of D4 and D1. That does not only impede the selection of key samples, because of missing predicted invariant reactions. Also a comparison of calculated phase boundaries to the DTA data in Table 2 and 3 would be misleading, which is revealed by considering the actual phases detected experimentally in the microstructures.

An accurate evaluation of the ternary Mg-Al-Ca system, including the ternary solubilities of the three Laves phases C14, C15, and C36, appears crucial for a correct calculation of quaternary and quinary phase relations. This was demonstrated for this ternary example with focus on phase equilibria involving (Mg). However, in other ternary systems the (Mg) phase is in equilibrium with numerous binary phases showing large ternary solubilities and even with ternary phases. This emphasizes the necessity of establishing proper ternary assessments before aiming at predictive quantitative calculations of quaternary and higher-order phase diagrams.

## 7. Conclusions

A procedure is suggested for identifying *key sample* compositions in *n*-component alloys, providing the most crucial information or the maximum return on the investment of experimental resources. The proposed algorithm

## Section I: Basic and Applied Research

furthermore establishes the exact type of reaction equation of the  $(n + 1)$  phase invariant equilibria.

Mg-Al-Ca-Sr alloys:

- A thermodynamic description for the quaternary system, developed from the four assessed ternary subsystems, is validated for alloys in equilibrium with (Mg).
- The two important five-phase reactions E1 and U8 predicted by the calculation are precisely confirmed by key experiments.
- Within the investigated composition range no quaternary compound exists. All four-component phases are binary phases with quaternary solubilities.
- The thermal signals from TA in the literature and from own DTA as well as the microstructure evolved during solidification are reproduced well by the thermodynamic predictions, as shown for both synthetic key alloys and a series of more Mg-rich alloys.

Mg-Al-Ca-Sr-Mn alloys:

- The consistent quaternary dataset is extended based on assessed descriptions of all four binary Mn-X systems and the Mg-Al-Mn system.
- Experimental results of quinary alloys support the predictive calculations, even for the unusual sample with more than 15 wt.% Mn, which is a key sample defining the most crucial invariant reaction involving (Mg).
- The existence of quaternary and quinary phases was checked but none was found.
- A consistent combination of ternary thermodynamic assessments may provide a reasonable database for calculation in higher-order alloys. This thesis is confirmed for the Mg-Al-Ca-Sr-Mn system. The impact of using less elaborate ternary data is also quantitatively exemplified. The necessity to establish proper ternary assessments before aiming at predictive quantitative calculations of quaternary and higher-order phase diagrams is emphasized.

### Acknowledgment

This study is supported by the German Research Foundation (DFG) in the Priority Programme “DFG-SPP 1168: InnoMagTec.”

### References

1. A. Janz and R. Schmid-Fetzer, Thermodynamics and Constitution of Mg-Al-Ca-Sr-Mn Alloys: Part I: Experimental Investigation and Thermodynamic Modeling of Subsystems Mg-Ca-Sr and Al-Ca-Sr, *J. Phase Equilib. Diffus.*, 2009 (accepted). doi:10.1007/s11669-009-9467-4
2. R. Schmid-Fetzer and J. Gröbner, Focused Development of Magnesium Alloys Using the Calphad Approach, *Adv. Eng. Mater.*, 2001, **3**, p 947-961
3. J. Ågren, F.H. Hayes, L. Höglund, U.R. Kattner, B. Legendre, and R. Schmid-Fetzer, Applications of Computational Thermodynamics, *Z. Metallkd.*, 2002, **93**, p 128-142
4. M. Ohno, D. Mirkovic, and R. Schmid-Fetzer, Liquidus and Solidus Temperatures of Mg-rich Mg-Al-Mn-Zn Alloys, *Acta Mater.*, 2006, **54**, p 3883-3891
5. A. Janz, J. Gröbner, D. Mirkovic, M. Medraj, J. Zhu, Y.A. Chang, and R. Schmid-Fetzer, Experimental Study and Thermodynamic Calculation of Al-Mg-Sr Phase Equilibria, *Intermetallics*, 2007, **15**(4), p 506-519
6. S.-L. Chen, S. Daniel, F. Zhang, Y.-A. Chang, X.-Y. Yan, F.-Y. Xie, R. Schmid-Fetzer, and W.-A. Oates, The Pandat Software Package and its Applications, *Calphad*, 2002, **26**, p 175-188
7. H.L. Lukas, E.-T. Henig, and G. Petzow, 50 Years Reaction Scheme After Erich Scheil, *Z. Metallkd.*, 1986, **77**, p 360-367
8. M. Ohno and R. Schmid-Fetzer, Thermodynamic Assessment of Mg-Al-Mn Phase Equilibria, Focusing on Mg-rich Alloys, *Z. Metallkd.*, 2005, **96**, p 857-869
9. A. Suzuki, N.D. Saddock, J.W. Jones, and T.M. Pollock, Solidification Paths and Eutectic Intermetallic Phases in Mg-Al-Ca Ternary Alloys, *Acta Mater.*, 2005, **53**, p 2823-2834
10. H. Cao, C. Zhang, J. Zhu, G. Cao, S. Kou, R. Schmid-Fetzer, and Y.A. Chang, Experiments Coupled with Modeling to Establish the Mg-rich Phase Equilibria of Mg-Al-Ca, *Acta Mater.*, 2008, **56**(18), p 5245-5254
11. A. Janz, J. Gröbner, H. Cao, J. Zhu, Y.A. Chang, and R. Schmid-Fetzer, Thermodynamic Modeling of the Mg-Al-Ca System, *Acta Mater.*, 2008, **57**(3), p 682-694
12. A. Janz, “Thermodynamics and Constitution of Quaternary Mg-Al-Ca-Sr Alloys and the Extension to the Quinary Mg-Al-Ca-Sr-Mn System,” Ph.D. thesis (Dr.-Ing., 28 March 2008), Clausthal University of Technology, Germany, 2008
13. Y. Du, J. Wang, J. Zhao, J.C. Schuster, F. Weitzer, R. Schmid-Fetzer, M. Ohno, H. Xu, Z.-K. Liu, S. Shang, and W. Zhang, Reassessment of the Al-Mn System and a Thermodynamic Description of the Al-Mg-Mn System, *Int. J. Mater. Res.*, 2007, **98**(9), p 855-871
14. U. Kattner, Thermodynamic Modeling of Multicomponent Phase Equilibria, *J. Mater.*, 1997, **49**, p 14-19
15. A. Suzuki, N.D. Saddock, L. Riester, E. Lara-Curzio, J.W. Jones, and T.M. Pollock, Effect of Sr Additions on the Microstructure and Strength of a Mg-Al-Ca Ternary Alloy, *Metall. Trans. A*, 2007, **38**(2), p 420-427
16. J. Gröbner, D. Kevorkov, I. Chumak, and R. Schmid-Fetzer, Experimental Investigation and Thermodynamic Calculation of Ternary Al-Ca-Mg Phase Equilibria, *Z. Metallkd.*, 2003, **94**, p 976-982
17. P. Liang, T. Tarfa, J.A. Robinson, S. Wagner, P. Ochin, M.G. Harmelin, H.J. Seifert, H.L. Lukas, and F. Aldinger, Experimental Investigation and Thermodynamic Calculation of the Al-Mg-Zn System, *Thermochim. Acta*, 1998, **314**, p 87-110
18. R. Agarwal, J. Lee, H. Lukas, and F. Sommer, Calorimetric Measurements and Thermodynamic Optimization of the Ca-Mg System, *Z. Metallkd.*, 1995, **86**(2), p 103-108
19. D. Kevorkov, R. Schmid-Fetzer, A. Pisch, F. Hodaj, and C. Colinet, The Al-Ca System, Part 2: Calorimetric Measurements and Thermodynamic Assessment, *Z. Metallkd.*, 2001, **92**, p 953-958
20. Y. Zhong, J.O. Sofo, A.A. Luo, and Z.-K. Liu, Thermodynamics Modeling of the Mg-Sr and Ca-Mg-Sr Systems, *J. Alloy. Compd.*, 2006, **421**, p 172-178
21. Y. Zhong, C. Wolverton, Y. Austin Chang, and Z.-K. Liu, A Combined CALPHAD/First-Principles Remodeling of the Thermodynamics of Al-Sr: Unsuspected Ground State Energies by

- “Rounding up the (Un)usual Suspects”, *Acta Mater.*, 2004, **52**, p 2739-2754
22. Y. Zhong, K. Ozturk, and Z.-K. Liu, Thermodynamic Modeling of the Ca-Sr-Zn Ternary System, *J. Phase Equilib.*, 2003, **24**, p 340-346
23. J. Gröbner, D. Mirkovic, M. Ohno, and R. Schmid-Fetzer, Experimental Investigation and Thermodynamic Calculation of Binary Mg-Mn Phase Equilibria, *J. Phase Equilib. Diffus.*, 2005, **26**, p 234-239
24. A. Kozlov, M. Ohno, R. Arroyave, Z.K. Liu, and R. Schmid-Fetzer, Phase Equilibria, Thermodynamics and Solidification Microstructures of Mg-Sn-Ca Alloys—Part 1. Experimental Investigation and Thermodynamic Modeling of the Ternary Mg-Sn-Ca System, *Intermetallics*, 2008, **16**(2), p 299-315